Article

Immunity

Transcription Factor IRF4 Promotes CD8$^+$ T Cell Exhaustion and Limits the Development of Memory-like T Cells during Chronic Infection

Graphical Abstract

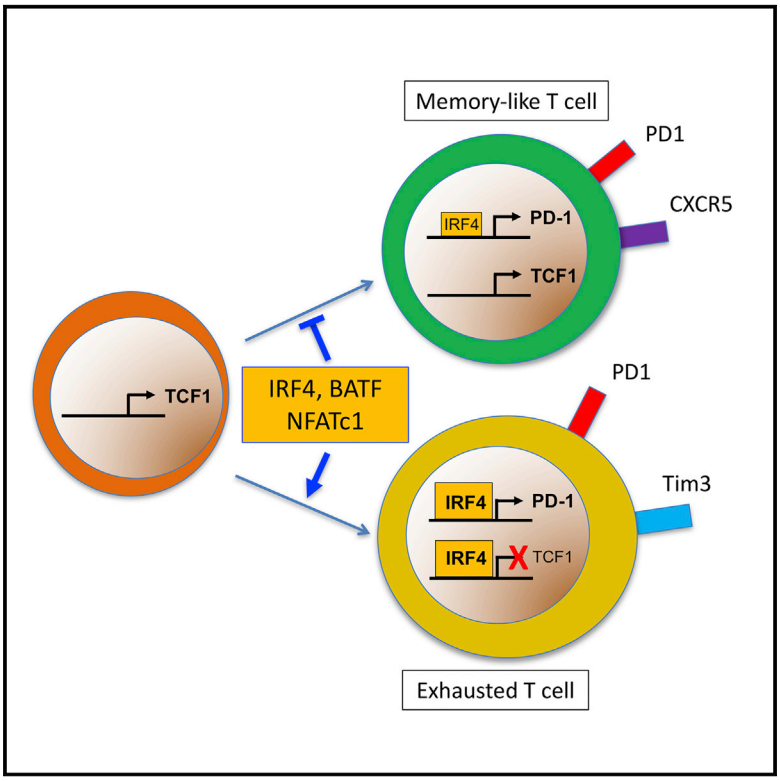

Highlights

- High IRF4 mediates T cell exhaustion including expression of inhibitory receptors
- TCR-responsive transcription factors IRF4, BATF, and NFAT form a transcriptional circuit
- Low IRF4 reduces T cell exhaustion and promotes formation of TCF1$^+$ memory-like T cells

Authors

Kevin Man, Sarah S. Gabriel, Yang Liao, ..., Mark A. Febbraio, Wei Shi, Axel Kallies

Correspondence

kallies@wehi.edu.au

In Brief

During chronic stimulation, CD8$^+$ T cells acquire an exhausted phenotype characterized by expression of inhibitory receptors, loss of effector function, and metabolic impairments. Man et al. have identified a transcriptional module consisting of the TCR-induced transcription factors IRF4, BATF, and NFATc1 that drives T cell exhaustion and impairs memory T cell development.

Man et al., 2017, Immunity *47*, 1129–1141
December 19, 2017
https://doi.org/10.1016/j.immuni.2017.11.021

CellPress

Immunity
Article

Transcription Factor IRF4 Promotes CD8+ T Cell Exhaustion and Limits the Development of Memory-like T Cells during Chronic Infection

Kevin Man,[1,2,10,11] Sarah S. Gabriel,[1,8,9,10] Yang Liao,[1,2] Renee Gloury,[1,8,9] Simon Preston,[1,2] Darren C. Henstridge,[3] Marc Pellegrini,[1,2] Dietmar Zehn,[4] Friederike Berberich-Siebelt,[5,6] Mark A. Febbraio,[7] Wei Shi,[1,2] and Axel Kallies[1,8,9,12,*]
[1]The Walter and Eliza Hall Institute of Medical Research, 1G Royal Parade, Parkville, VIC 3052, Australia
[2]The Department of Medical Biology, University of Melbourne, Parkville, VIC 3010, Australia
[3]Baker Heart and Diabetes Institute, Melbourne, VIC 3004, Australia
[4]Division of Animal Physiology and Immunology, School of Life Sciences Weihenstephan, Technical University of Munich, 85354 Freising, Germany
[5]Institute of Pathology, University of Würzburg, 97080 Würzburg, Germany
[6]Comprehensive Cancer Center Mainfranken, University of Würzburg, 97080 Würzburg, Germany
[7]Cellular and Molecular Metabolism, Garvan Institute, Sydney, NSW 2010, Australia
[8]Department of Microbiology and Immunology, The University of Melbourne, Parkville, VIC 3010, Australia
[9]The Peter Doherty Institute for Infection and Immunity, University of Melbourne, Melbourne, VIC 3000, Australia
[10]These authors contributed equally
[11]Present address: Cardiovascular Research Institute, University of California, San Francisco, CA 94143, USA
[12]Lead Author
*Correspondence: kallies@wehi.edu.au
https://doi.org/10.1016/j.immuni.2017.11.021

SUMMARY

During chronic stimulation, CD8+ T cells acquire an exhausted phenotype characterized by expression of inhibitory receptors, down-modulation of effector function, and metabolic impairments. T cell exhaustion protects from excessive immunopathology but limits clearance of virus-infected or tumor cells. We transcriptionally profiled antigen-specific T cells from mice infected with lymphocytic choriomeningitis virus strains that cause acute or chronic disease. T cell exhaustion during chronic infection was driven by high amounts of T cell receptor (TCR)-induced transcription factors IRF4, BATF, and NFATc1. These regulators promoted expression of inhibitory receptors, including PD-1, and mediated impaired cellular metabolism. Furthermore, they repressed the expression of TCF1, a transcription factor required for memory T cell differentiation. Reducing IRF4 expression restored the functional and metabolic properties of antigen-specific T cells and promoted memory-like T cell development. These findings indicate that IRF4 functions as a central node in a TCR-responsive transcriptional circuit that establishes and sustains T cell exhaustion during chronic infection.

INTRODUCTION

T cells responding to persistent viral or tumor antigens acquire an altered state of differentiation referred to as "exhaustion" that is defined by the progressive loss of effector function and impaired memory T cell potential (Virgin et al., 2009; Speiser et al., 2014; Kahan et al., 2015; Wherry and Kurachi, 2015). Exhausted T cells successively lose their ability to produce cytokines, including interferon-gamma (IFN-γ), tumor necrosis factor (TNF), and interleukin-2 (IL-2), and exhibit impaired survival, eventually leading to the deletion of antigen-specific cells. They express multiple inhibitory receptors, including programmed cell-death 1 (PD-1), lymphocyte-activation gene 3 (Lag3), TIM-3, CTLA4, TIGIT, and 2B4, associated with functional impairments. Conversely, inhibitory receptors are required to prevent overt immune pathology due to chronic stimulation of antigen-specific T cells (Blackburn et al., 2009; Virgin et al., 2009; Speiser et al., 2014; Kahan et al., 2015; Wherry and Kurachi, 2015). For example, PD-1 binding to either PD ligand (PD-L)1 or PD-L2 facilitates the dephosphorylation of key proteins downstream of the T cell receptor (TCR), leading to the inhibition of TCR-dependent signal transduction (Keir et al., 2008). T cell exhaustion has recently been linked to defects in cellular metabolism (Gubin et al., 2014; Staron et al., 2014; Bengsch et al., 2016; Schurich et al., 2016), which has emerged as a major checkpoint in adaptive immune responses (Pearce et al., 2013; Wang and Green, 2012). Indeed, compromised metabolic fitness is closely linked to the functional impairments of tumor-infiltrating T cells that frequently display an exhausted phenotype (Chang et al., 2015; Ho et al., 2015). Recently, PD-1 signaling was shown to directly contribute to establishing the metabolic impairments of exhausted T cells (Bengsch et al., 2016), suggesting that exhaustion is underpinned by substantial rewiring of TCR signaling-mediated metabolic processes.

Several studies have demonstrated that exhausted T cells are characterized by a transcriptional program that is distinct from effector and memory T cells that arise during acute infection (Wherry et al., 2007; Doering et al., 2012; Kahan et al., 2015).

A number of key transcription factors were identified that control the degree of exhaustion during chronic infection, including T-bet (encoded by *Tbx21*), Blimp-1 (encoded by *Prdm1*), Eomesodermin (Eomes), von Hippel-Lindau tumor suppressor (VHL), and Foxo1 (Shin et al., 2009; Kao et al., 2011; Paley et al., 2012; Doedens et al., 2013; Staron et al., 2014). Recently, the transcriptional regulators TCF1, BCL6, Blimp-1, and Id2 and Id3 (via binding to E2A) were found to control the regenerative and migratory capacities of exhausted T cells (He et al., 2016; Im et al., 2016; Leong et al., 2016; Utzschneider et al., 2016). Thus, multiple transcription factors are co-opted in transcriptional modules that differ between acute and chronic infection. However, the molecular network that initiates, drives, and sustains the functional impairments of exhausted cells is incompletely known.

To further unravel the transcriptional circuits that underlie the establishment of functional and metabolic exhaustion of T cells, we here performed transcriptional profiling of antigen-specific $CD8^+$ T cells isolated from mice infected with two different strains of lymphocytic choriomeningitis virus (LCMV) causing acute and chronic infections, respectively. We demonstrate that exhausted T cells in comparison to fully functional effector and memory T cells expressed elevated amounts of the TCR-responsive transcription factors IRF4 and BATF, which promoted the expression of multiple inhibitory receptors including PD-1, impaired effector function, and repressed anabolic metabolism. Furthermore, exhausted T cells expressed high amounts of transcription factor NFATc1, and both NFATc1 and NFATc2 were required for the TCR-dependent induction of IRF4. Genome-wide occupancy of IRF4, BATF, and NFAT was enriched at genes that constituted the exhaustion-specific gene signature. Reduction of IRF4 expression was sufficient to restore anabolic metabolism and favored the formation of TCF1-expressing memory-like antigen-specific T cells. Overall our data demonstrate that TCR-responsive transcription factors cooperatively establish T cell exhaustion while repressing memory T cell characteristics during chronic viral infection.

RESULTS

Exhausted T Cells Express Elevated Amounts of IRF4 and BATF

To identify molecular mechanisms underlying the distinct properties of exhausted T cells, we performed RNA sequencing (RNA-seq) analyses on adoptively transferred P14 TCR transgenic $CD8^+$ T cells recognizing the LCMV glycoprotein (gp)-derived epitope gp33-41 (gp33) isolated from mice infected with two different strains of LCMV, causing either an acute (WE) or chronic (Docile) infection. In agreement with earlier reports (Doering et al., 2012; Wherry et al., 2007), we observed pronounced differences between the transcriptional profiles of acutely stimulated and exhausted T cells. We identified 945 genes early (day 8) and 1,529 genes late (day 30) specifically up- or downregulated in chronically stimulated cells in comparison to acutely stimulated cells (>1.5-fold, <0.1 FDR). This set comprised a total of 2,050 unique "chronic $CD8^+$ T cell signature" genes, of which 826 showed a differential expression of >2-fold (Figure 1A and Table S1). This included several genes encoding inhibitory receptors, including *Pdcd1* (PD-1), *Havcr2* (TIM-3), *Tigit*, and others, which were strongly upregulated in exhausted T cells, as well as transcription factors known to be important for the differentiation of exhausted or memory T cells such as *Prdm1* (Blimp1), *Eomes*, and *Tcf7* (TCF1) (Figures 1B and 1C). In addition, our RNA-seq data revealed that exhausted T cells in comparison to acutely stimulated T cells expressed high amounts of *Irf4* mRNA, encoding a transcription factor that integrates TCR signaling with cellular metabolism and clonal population expansion of effector $CD8^+$ T cells (Man and Kallies, 2015; Man et al., 2013). High IRF4 expression in antigen-specific $CD8^+$ T cells in mice infected with chronic LCMV Docile as compared to mice infected with acute LCMV WE was confirmed by quantitative PCR and intracellular staining, showing that high IRF4 protein expression was established early in chronically stimulated T cells and was maintained up to at least 30 days after establishment of chronic infection (Figures 1D and 1E). Exhausted T cells compared to acutely stimulated T cells also expressed elevated amounts of the AP-1 transcription factor BATF (Figures 1F and 1G) that is required for efficient DNA binding and transcriptional activity of IRF4 in T cells (Glasmacher et al., 2012; Li et al., 2012). Expression of both IRF4 and BATF tightly correlated with high expression of PD-1 in P14 T cells (Figures 1H and 1I). Thus, T cell exhaustion is characterized by the elevated expression of the two TCR-responsive transcription factors IRF4 and BATF.

High Amounts of IRF4 Drive T Cell Exhaustion

To examine the role of IRF4 in T cell exhaustion, we generated mice carrying floxed *Irf4* alleles on a *Cd4Cre* transgenic background, resulting in conditional ablation of *Irf4* in all T cells. As previously reported in the setting of acute infection (Man et al., 2013; Yao et al., 2013), complete loss of IRF4 in T cells in chronically infected $Irf4^{fl/fl}Cd4Cre$ mice resulted in severely impaired population expansion of gp33 and nucleoprotein (NP)396 LCMV epitope-specific $CD8^+$ T cells and diminished viral control (Figures S1A and S1B). To test a potential link between IRF4 dose and exhaustion, we infected mice in which only one copy of *Irf4* was deleted in T cells ($Irf4^{fl/+}Cd4Cre$). Loss of one *Irf4* allele resulted in decreased numbers of antigen-specific $CD8^+$ T cells compared to controls (Figure S1C). Notably, however, viral control was not affected (Figure S1D), suggesting that the remaining antigen-specific T cells were functionally superior compared to their wild-type (WT) counterparts.

To examine the potential link between IRF4, inhibitory receptor expression, and functionality of antigen-specific T cells in more detail, we co-transferred congenically marked WT and $Irf4^{+/-}$ P14 T cells into recipient mice, which we infected with chronic LCMV Docile. Co-transfer of the cells ensured that both WT and $Irf4^{+/-}$ $CD8^+$ T cells were exposed to the same viral load and inflammation. $Irf4^{+/-}$ P14 T cells expressed reduced amounts of IRF4 protein (Figure S1E) and were substantially impaired in their ability to undergo clonal population expansion (Figure 2A). However, $Irf4^{+/-}$ P14 T cells secreted increased amounts of cytokines IFN-γ, TNF, and IL-2 (Figures 2B and 2C) and displayed reduced expression of inhibitory receptors PD-1, TIM-3, Lag3, 2B4, TIGIT, and CTLA4 (Figures 2D and 2E) compared to their WT counterparts, which could be reversed by overexpression of IRF4 (Figure S1F). Mice that received $Irf4^{+/-}$ P14 T cells showed a more pronounced drop in core

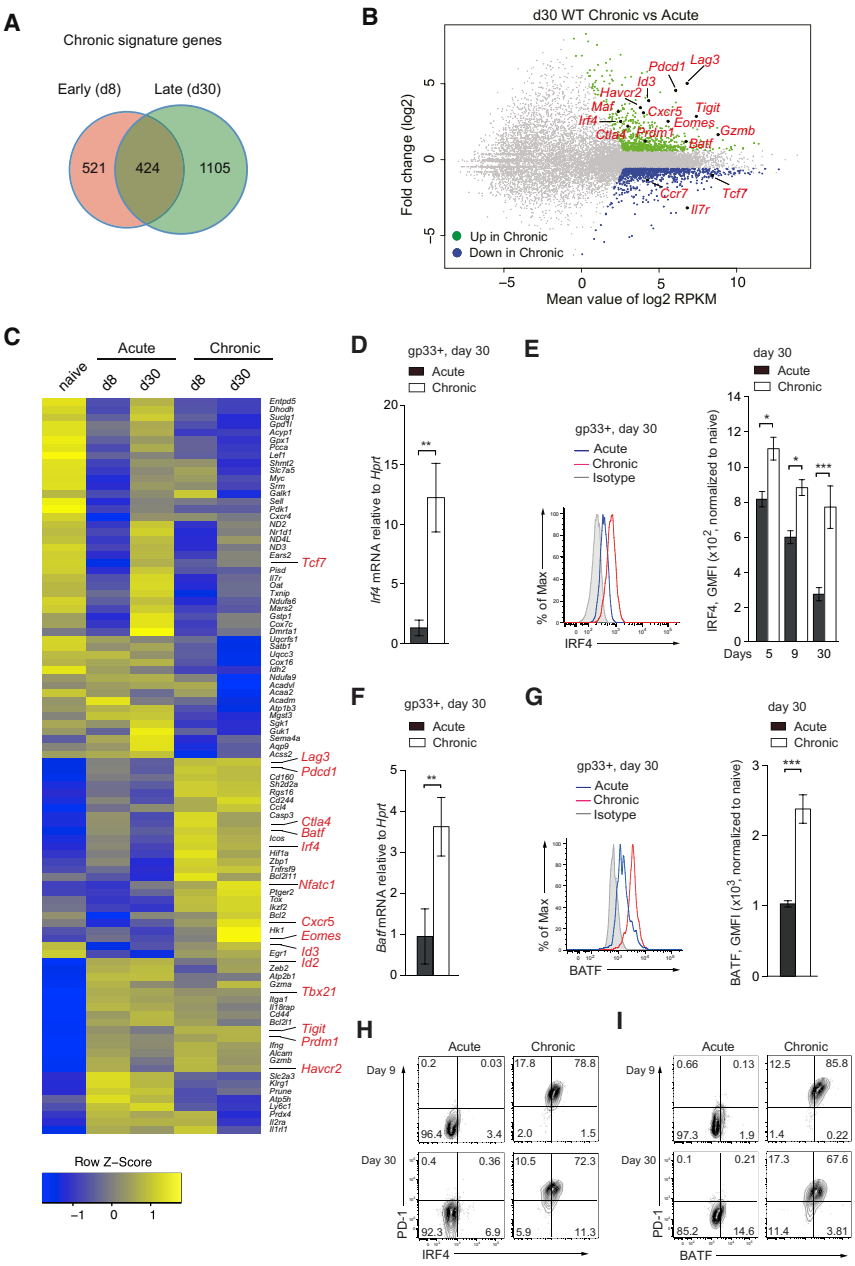

Figure 1. Exhausted T Cells Express Elevated Levels of the Transcription Factors IRF4 and BATF

Transcriptional profiling (RNA sequencing) was performed on antigen-specific P14 T cells isolated from mice infected with LCMV strains causing acute (WE) or chronic (Docile) infections.

(A) Venn diagram showing overlap between genes that display significant changes (>1.5-fold, < 0.1 FDR) in expression between P14 T cells isolated from mice infected with chronic LCMV compared to P14 T cells isolated from mice infected with acute LCMV, early (day 8) or late (day 30) post infection (p.i.).

(B) MA plot showing genes downregulated (blue) or upregulated (green) in chronically versus acutely stimulated T cells at day 30 p.i. Key genes of interest are indicated.

(C) Heatmap displaying expression of selected "chronic $CD8^+$ T cell signature" genes as in (A). Shown are genes encoding inhibitory receptors, transcriptional regulators, and chemokine receptors previously implicated in T cell exhaustion (Doering et al., 2012; Kahan et al., 2015; Wherry et al., 2007). Naive P14 T cells were included for comparison.

(D) Quantitative RT-PCR analysis of *Irf4* mRNA expression in flow cytometry-sorted gp33-specific T cells from acutely and chronically LMCV-infected mice relative to *Hprt* expression at day 30 p.i.

(E) Histogram (day 30 p.i., left) and geometric mean fluorescence intensity (GMFI) of IRF4 expression in gp33-specific T cells from mice infected with acute or chronic LCMV, assessed by intracellular staining at indicated times p.i. (right). GMFI is normalized to IRF4 expression in naive T cells.

(F) Quantitative RT-PCR analysis of *Batf* mRNA expression in flow cytometry-sorted gp33-specific T cells from acutely and chronically LCMV-infected mice relative to *Hprt* expression at day 30 p.i.

(G) BATF expression assessed by intracellular staining in gp-33-specific T cells 30 days after chronic or acute LCMV infection. GMFI is normalized to BATF expression in naive T cells (right).

(H and I) P14 cells from acutely or chronically LCMV-infected mice stained for PD-1 and IRF4 (H), or PD-1 and BATF (I) and analyzed by flow cytometry at day 9 and day 30 p.i.

Error bars denote mean ± SEM. Graphs in (D)–(I) are representative of 3–4 independent experiments with 4–5 mice per group. Statistical analysis was performed using unpaired two-tailed Student's t test (*$p < 0.05$, **$p < 0.01$, ***$p < 0.001$).

body temperature (Figure 2F) and augmented cellular infiltration into multiple non-lymphoid organs as compared to mice harboring only WT P14 T cells (Figure S1G); however, viral clearance was not improved (Figure S1H). Similar results were obtained from chronically infected bone marrow chimeric mice, showing impaired population expansion and reduced expression of inhibitory receptors of endogenous *Irf4*$^{+/-}$ and *Irf4*$^{-/-}$ antigen-specific $CD8^+$ T cells in comparison to their WT counterparts (Figures S2A–S2C). Tamoxifen-induced deletion of IRF4 from *Irf4*$^{fl/fl}$*Cre*^{ERT2} T cells during the chronic phase of the infection resulted in dramatic loss of antigen-specific T cells and a reduction in PD-1 expression, indicating that IRF4 was required not only for the initial expansion of antigen-specific T cells but also for maintaining their numbers and phenotype during an ongoing chronic infection (Figure 2G).

BATF and IRF4 have been shown to cooperate in the differentiation of effector $CD8^+$ T cells (Man et al., 2013; Kurachi et al., 2014). Reduction or loss of BATF also resulted in reduced expression of multiple inhibitory receptors in gp33-specific T cells from chronically LCMV-infected bone marrow chimeric mice (Figures 2H and S2D). Consistent with this result, *Batf*$^{+/-}$ P14 T cells isolated from chronically LCMV-infected mice showed increased production of IFN-γ, but not TNF or IL-2, compared to their wild-type counterparts isolated from the same mice (Figure S2E). Overall, these data indicate that high amounts of IRF4 and BATF are required for the population expansion and maintenance of

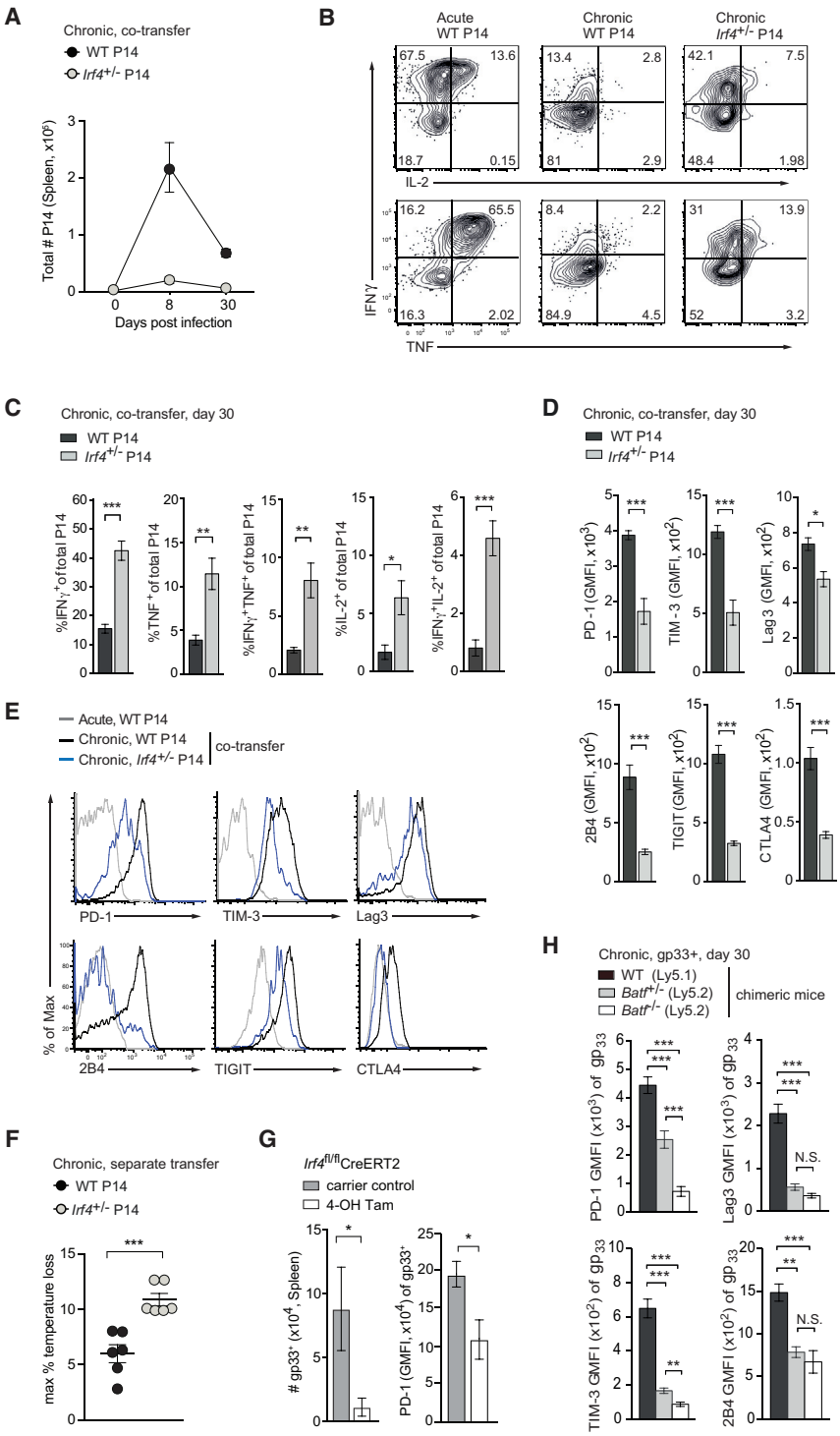

Figure 2. IRF4 Drives T Cell Exhaustion and Restrains Effector Function

Congenically marked wild-type (WT, Ly5.1) and *Irf4*$^{+/-}$ (Ly5.2) P14 T cells were co-transferred into recipient mice (Ly5.1^{+}Ly5.2^{+}), which were infected with acute (WE) or chronic LCMV (Docile) subsequently.

(A) Absolute numbers of adoptively co-transferred WT and *Irf4*$^{+/-}$ P14 T cells over the course of a chronic LCMV infection.

(B and C) Representative flow cytometric analysis (B) and quantification (C) of IFN-γ, TNF, and IL-2 expression in WT and *Irf4*$^{+/-}$ P14 T cells following *ex vivo* gp33 peptide restimulation at day 30 post infection (p.i.).

(D and E) Geometric mean fluorescence intensity (GMFI, D) and representative (E) histograms of PD-1, TIM-3, Lag3, 2B4, TIGIT, and CTLA4 expression on WT and *Irf4*$^{+/-}$ P14 T cells at day 30 after chronic LCMV infection. Histograms representing P14 in acute infection are shown in (E) as a reference.

(F) Maximum drop of core body temperature of chronically LCMV-infected mice that received WT or *Irf4*$^{+/-}$ P14 T cells. Donor cell numbers were adjusted to achieve similar representation of WT and *Irf4*$^{+/-}$ P14 cells, respectively, at day 13 p.i.

(G) Absolute numbers (left) and PD-1 expression (right) of gp33-specific CD8^{+} T cells in *Irf4*$^{fl/fl}$ mice carrying a tamoxifen-inducible Cre recombinase transgene (ERT2 Cre) after deletion of IRF4 using 4-OH tamoxifen (4-OH Tam) or control treatment with carrier only (peanut oil). Mice were treated at day 15 and analyzed at day 30 after chronic LCMV infection.

(H) GMFI of inhibitory receptors PD-1, Lag3, TIM-3, and 2B4 on gp33-specific CD8 T cells in chronically LCMV-infected bone marrow chimeric mice reconstituted with WT and *Batf*$^{+/-}$ or WT and *Batf*$^{-/-}$ hematopoietic cells at day 30 p.i.

Flow cytometry data in (B) and (E) are representative and data in (C) and (D) are pooled from 2 independent experiments with 4–6 mice per group. Data in (F) are representative of 2 independent experiments, containing 3–6 mice per group, and data in (G) are representative of 2 experiments with 3–4 mice each. Data in (H) are pooled from 3 independent experiments with 3–5 mice per group. Error bars denote mean ± SEM and statistical analysis was performed using paired (H) or unpaired two-tailed (all other) Student's t test (*$p < 0.05$, **$p < 0.01$, ***$p < 0.001$).

antigen-specific T cells during chronic infection, while promoting T cell exhaustion at the same time.

IRF4 Suppresses Anabolic Metabolism and Mitochondrial Function in Exhausted T Cells

Further analysis of the RNA-seq data showed that metabolic pathways were significantly enriched among chronic signature genes (Figures S3A and S3B, Table S2). Consistent with this finding, chronically stimulated T cells showed reduced mitochondrial membrane potential and mass, exhibited increased oxygen consumption rate (OCR) utilized for ATP production, and displayed an increased proton leak (Figures 3A and 3B), indicating decreased efficiency of coupled respiration. Chronically stimulated T cells, in particular PD-1^{hi} cells, showed reduced production of reactive oxygen species (ROS), a byproduct of electron transport chain-dependent respiration (Figures 3C and 3D) that is critical for cellular activation

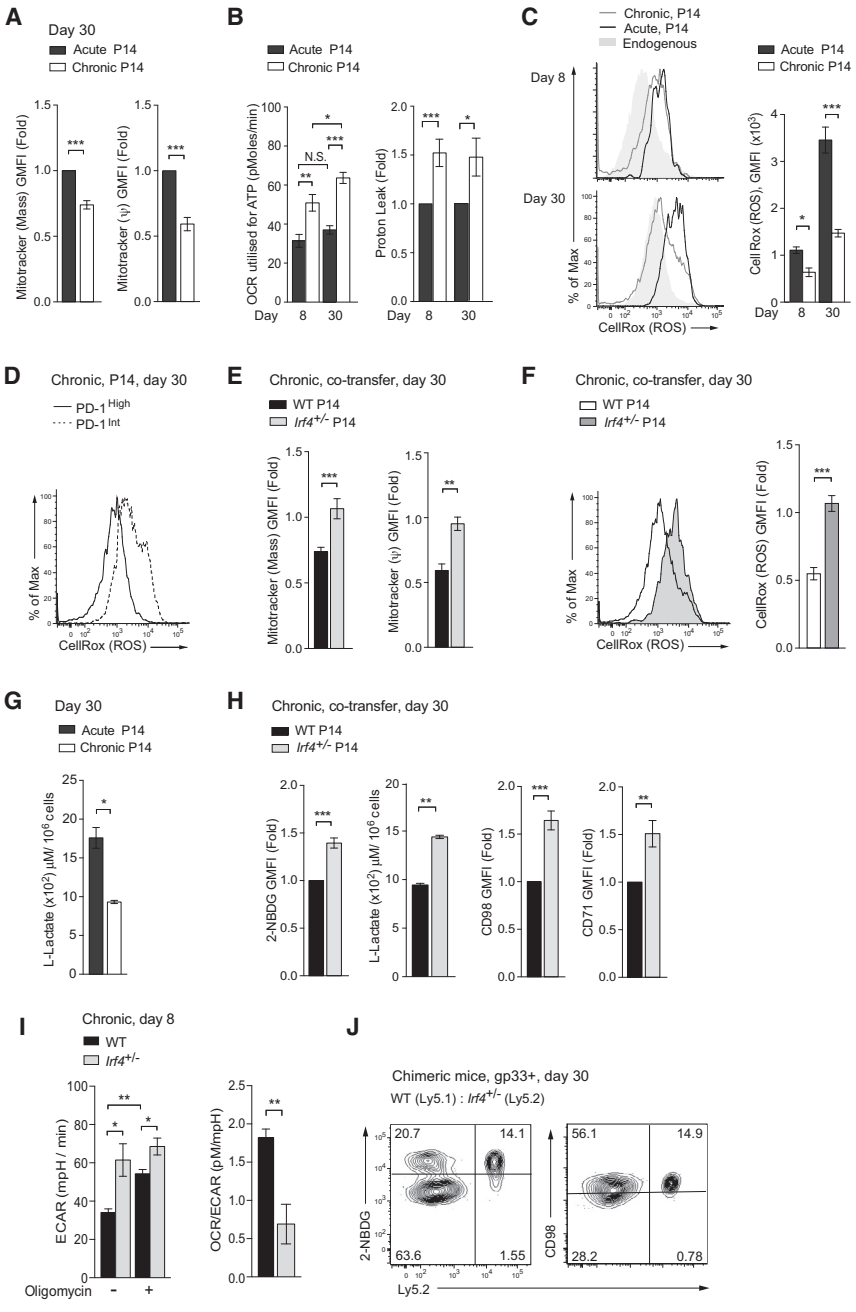

Figure 3. IRF4 Drives Bioenergetic Insufficiencies during T Cell Exhaustion

(A) Mitochondrial mass and membrane potential determined by Mitotracker Green and Mitotracker Orange (CMTMRos) labeling, respectively, in P14 T cells isolated from acutely (WE) or chronically (Docile) LCMV-infected mice at day 30 post infection (p.i). Geometric mean fluorescence intensity (GMFI) was normalized to GMFI in P14 cells isolated from acute LCMV infection.

(B) Oxygen consumption rate (OCR) utilized for ATP turnover calculated as the difference in basal rate and rate following oligomycin treatment (left), and proton leak (right) calculated as the difference between OCR after oligomycin and after rotenone/antimycin and expressed as fold change over P14 T cells in acute infection at days 8 and 30 p.i.

(C) Representative histograms (left) and corresponding GMFI (right) of reactive oxygen species (ROS) abundance determined by CellRox DeepRed labeling in adoptively transferred P14 T cells during acute and chronic LCMV infection at days 8 and 30 p.i.

(D) ROS abundance determined by CellRox DeepRed labeling in PD-1 high and PD-1 intermediate (int) P14 T cells in chronically LCMV-infected mice at day 30 p.i.

(E and F) Congenically marked wild-type (WT, Ly5.1) and *Irf4*$^{+/-}$ (Ly5.2) P14 T cells were co-transferred into Ly5.1^{+}Ly5.2^{+} hosts and analyzed at day 30 after chronic LCMV infection. Mitochondrial mass and membrane potential were determined by Mitotracker Green and Mitotracker Orange (CMTMRos) labeling (E). ROS abundance was determined by CellRox DeepRed labeling (F). Normalized to GMFI of WT P14 from acute LCMV infection at day 30 p.i.

(G) Extracellular L-Lactate production from flow cytometry-sorted P14 cells at day 30 after acute or chronic LCMV infection and stimulated *ex vivo* with IL-2.

(H) Uptake of fluorescent glucose analog 2-NBDG, extracellular L-Lactate production after *ex vivo* stimulation with IL-2, and expression of CD98 and CD71 (GMFI normalized to WT P14 cells) in WT and *Irf4*$^{+/-}$ P14 cells as (E).

(I) Basal extracellular acidification rate (ECAR) measured on bulk effector phenotype (CD62L^{-}CD44^{+}) CD8^{+} T cells isolated from WT or *Irf4*$^{+/-}$ mice at day 8 after chronic LCMV infection with and without the addition of oligomycin (left) and the OCR/ECAR ratio (right).

(J) Representative flow cytometric analysis of fluorescent glucose analog 2-NBDG uptake and expression of CD98 on congenically marked WT (Ly5.1) and *Irf4*$^{+/-}$ (Ly5.2) gp33-specific CD8^{+} T cells from mixed bone marrow chimeric mice infected with chronic LCMV and analyzed at day 30 p.i.

Data in (A), (C), (E), and (H) are pooled from 2–4 independent experiments with 3–4 mice per group; other data are representative of 2–4 independent experiments with 3–4 mice per group. Error bars denote mean ± SEM and statistical analysis was performed using unpaired two-tailed Student's t test (*p < 0.05, **p < 0.01, ***p < 0.001).

and for the maintenance of cytotoxic T cell proliferation and function (Sena et al., 2013; Weinberg et al., 2015). Reducing the amount of IRF4 in chronically stimulated P14 T cells was sufficient to restore mitochondrial size and membrane potential as well as ROS production (Figures 3E and 3F). Consistent with impaired anabolic metabolism, chronically stimulated P14 T cells in response to stimulation with IL-2 secreted less L-Lactate, an end-product of aerobic glycolysis (Figure 3G). In contrast, *Irf4*$^{+/-}$ P14 T cells responding to chronic LCMV infection showed increased uptake of the glucose analog 2-NBDG, secreted elevated amounts of L-Lactate, and showed increased expression of the amino acid transporter component CD98 and the transferrin receptor CD71 (Figure 3H), which could be reverted by overexpression of IRF4 (Figure S3C). Indeed, as early

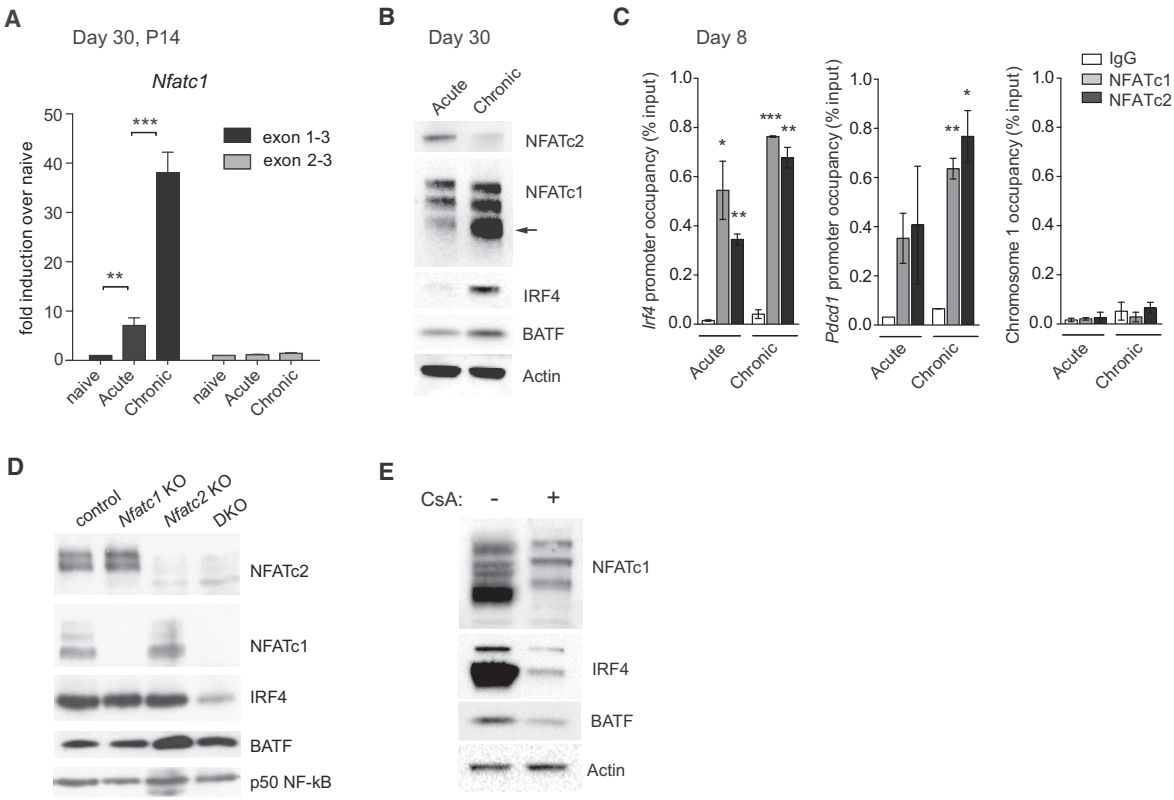

Figure 4. IRF4 and NFAT Form a Positive Feedback Circuit during T Cell Exhaustion

(A) Expression of *Nfatc1* isoforms as identified by RNA sequencing. Graph shows expression relative to naive T cells of the short isoform (NFATc1aA, represented by exon 1–3 junctions, skipping exon 2) and the long isoform (represented by exon 2–3 junctions) in P14 T cells isolated from acutely (WE) and chronically (Docile) LCMV-infected mice at day 30 post infection (p.i.).

(B) Western blot showing NFATc1, NFATc2, IRF4, BATF, and Actin (loading control) expression in $CD8^+$ T cells flow cytometry sorted as $CD62L^-$ from acutely and as $CD62L^-PD\text{-}1^+$ from chronically LCMV-infected mice at day 30 p.i. The arrow marks the short isoform of NFATc1.

(C) Binding of NFATc1 and NFATc2 to the *Irf4* and *Pdcd1* (encoding PD-1) promoters demonstrated by chromatin immunoprecipitation using specific antibodies or control IgG and RT-qPCR in total $CD44^+CD8^+$ T cells isolated from spleens of acutely and chronically LCMV-infected mice at day 8 p.i. Enrichment is expressed as percentage of total chromatin input and compares isotype control and NFATc1- and NFATc2-specific antibodies.

(D) Western blot showing NFATc1, NFATc2, IRF4, BATF, and p50 NF-κB (loading control) expression in polyclonal $CD8^+$ T cells deficient (KO) in NFATc1 (*Nfatc1*$^{fl/fl}$*Cd4Cre*), NFATc2 (*Nfatc2*$^{-/-}$), or both (DKO) after *in vitro* activation with anti-CD3 and anti-CD28 for 48 hr.

(E) Western blot showing NFATc1, IRF4, BATF, and Actin (loading control) in polyclonal $CD8^+$ T cells activated with anti-CD3, anti-CD28, and IL-2 with or without cyclosporine A (CsA) for 24 hr.

Data in (A)–(C) are representative of 2 independent experiments and data in (D) and (E) are representative of 3 independent experiments. Error bars denote mean ± SEM. Statistical analysis was performed using unpaired two-tailed Student's t test (*$p < 0.05$, **$p < 0.01$, ***$p < 0.001$).

as day 8 during chronic infection, bulk *Irf4*$^{+/-}$ effector $CD8^+$ T cells showed elevated extracellular acidification rate (ECAR) and a pronounced shift in the OCR to ECAR ratio in comparison to their WT counterparts (Figure 3I). Similar results were obtained from endogenous *Irf4*$^{+/-}$ gp33-specific $CD8^+$ T cells from LCMV Docile-infected mixed bone marrow chimeric mice (Figures 3J, S3D, and S3E). Collectively, these data indicate that increased expression of IRF4 contributes to the suppression of glycolysis and OXPHOS in exhausted T cells.

IRF4 and NFAT Form a Positive Feedback Circuit during T Cell Exhaustion

Induction of inhibitory receptor expression is mediated by the transcription factors NFATc1 and NFATc2 (Lu et al., 2014; Martinez et al., 2015; Oestreich et al., 2008). In line with this notion, we found that exhausted T cells expressed elevated amounts of *Nfatc1* RNA, in particular the short isoform *Nfatc1aA* (Figure 4A), which is transcriptionally induced by TCR signaling and utilizes exon 1 and an intragenic 3′ UTR (Serfling et al., 2012). Accordingly, high amounts of NFATc1 protein were expressed together with IRF4 and BATF, whereas NFATc2 showed reduced abundance in effector $CD8^+$ T cells from LCMV Docile in comparison to WE-infected mice (Figure 4B). Chromatin immunoprecipitation (ChIP) and quantitative RT-PCR showed that NFATc1 and NFATc2 binding was enriched in the promoter regions of the *Irf4* and *Pdcd1* loci in $CD8^+$ T cells isolated from acutely or chronically LCMV-infected mice compared to isotype controls (Figure 4C). Notably, combined ablation of *Nfatc1* and *Nfatc2* resulted in a substantial reduction of IRF4 but not BATF in activated $CD8^+$ T cells (Figure 4D). In line with a critical role for NFAT proteins in the induction of IRF4 expression, $CD8^+$ T cells activated in the presence of cyclosporine A, an inhibitor

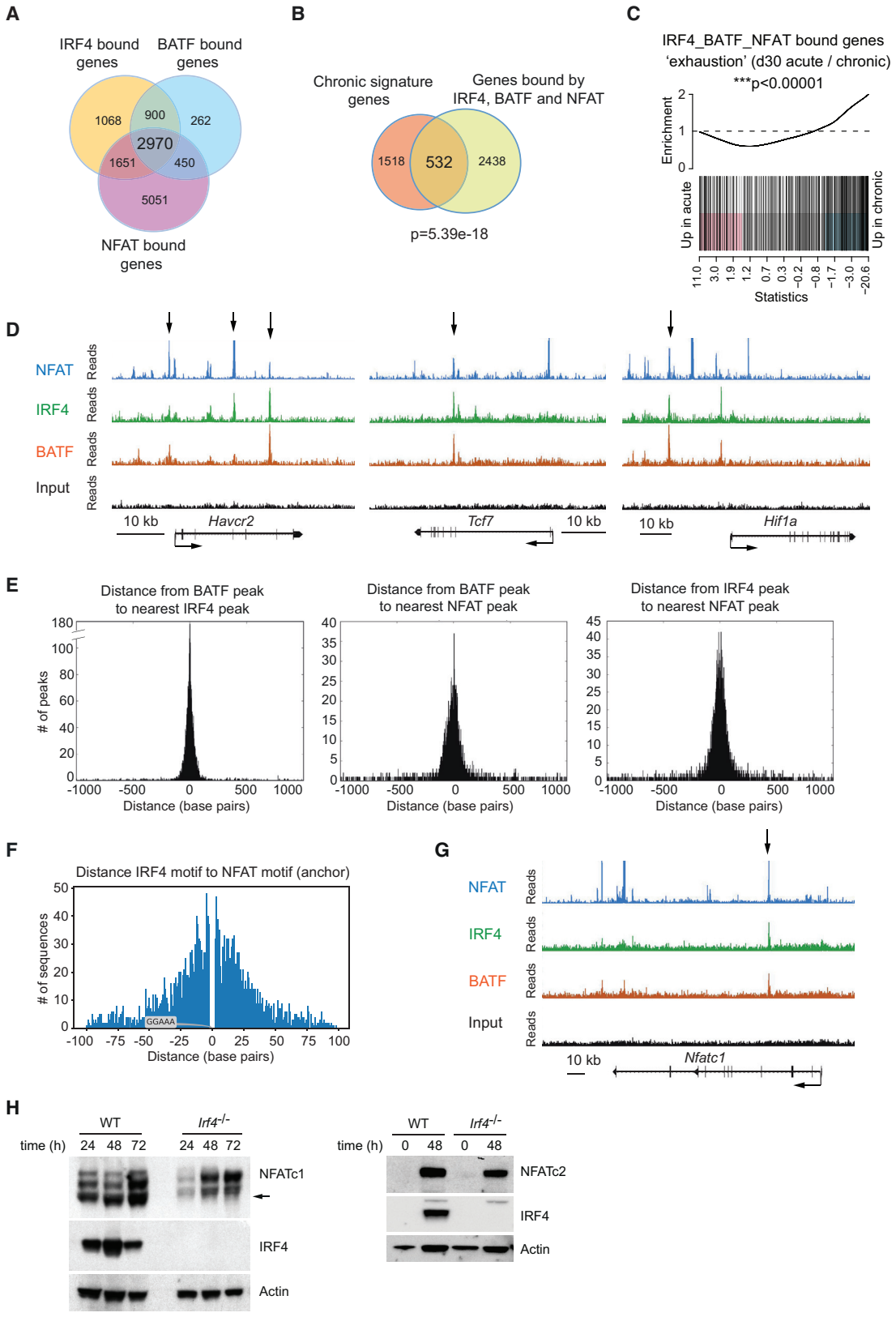

Figure 5. IRF4 and BATF Cooperate with NFAT to Establish T Cell Exhaustion

(A) Venn diagram showing overlap between genes bound by IRF4, BATF, and NFAT as identified by chromatin immunoprecipitation (ChIP) sequencing of effector CD8$^+$ T cells (Kurachi et al., 2014; Man et al., 2013; Martinez et al., 2015).

(legend continued on next page)

of NFAT activity, expressed very little IRF4 protein and showed reduced expression of BATF (Figure 4E). Overall, these data indicate that NFATs are major inducers of IRF4 expression and show that elevated expression of NFAT, in particular NFATc1, contributes to the increased expression of IRF4 and BATF in chronically stimulated T cells.

IRF4 and BATF Cooperate with NFAT to Establish T Cell Exhaustion

To understand how the elevated expression of multiple TCR-responsive transcription factors contributes to the establishment of T cell exhaustion, we examined genome-wide DNA binding data for IRF4, BATF, and NFAT (Man et al., 2013; Kurachi et al., 2014; Martinez et al., 2015). IRF4, BATF, and NFAT shared a large proportion of their target genes (Figure 5A). Binding of all three factors was significantly enriched among genes encoding transcripts that constituted the chronic signature (Figures 5B and 5C) and included genes encoding inhibitory receptors (e.g., *Pdcd1*, *Havcr2*, *Ctla4*), molecules involved in cellular metabolism (e.g., *Hif1a*, *Slc2a3*, *Pgm2l1*), mitochondrial electron transport chain complex components (e.g., *Atp2c1*, *Atp7a*, *Atp10a*, *Ndufv2*, *Ndufaf2*), and effector and memory T cell development (*Tcf7*, *Foxo1*, *Tbx21*, *Prdm1*) (Figures 5D, S4A, and S4B, Table S3). This was in contrast to genes bound by only one or two of the transcription factors, which showed no or little enrichment among the chronic signature genes (Figure S4C).

Genome-wide, BATF and IRF4 binding sites were enriched in close proximity to each other, while NFAT sites were enriched adjacent to both BATF and IRF4 sites (Figure 5E). Indeed, the IRF4 motif was found to be enriched in close proximity to the core NFAT motif, with 50% of the IRF4 motifs located in $\leq$23 bp distance to the NFAT motif (Figure 5F). Similar enrichment was observed for the AP-1 motif (recognized by BATF), with 50% of the IRF4 and NFAT motifs located in $\leq$20 bp distance to the AP-1 motif (Figure S5A), as shown for the composite intronic binding site in *Tcf7* (Figure S5B). Overall, we detected overlapping ChIP-seq peaks (mean overlap >113 bp) at 2,185 sites, providing evidence for co-binding of all three transcription factors. The AP-1 core motif (TGAnTCA) was the most enriched motif within these regions (Figure S5C). Interestingly, we found that IRF4 together with BATF and NFAT itself bound to the *Nfatc1* locus (Figure 5G), suggesting a feedback loop regulated by the activity of all three transcription factors. Indeed, *Irf4*$^{-/-}$ CD8$^+$ T cells showed reduced expression of NFATc1, in particular the short isoform, but not of NFATc2 (Figure 5H). Overall, our data indicate that NFAT, IRF4, and BATF cooperate at key genomic loci that control the transcriptional signature of exhausted T cells.

IRF4 Controls the Transcriptional Profile Associated with Exhaustion

To understand how high amounts of IRF4 drive T cell exhaustion, we performed transcriptional profiling of *Irf4*$^{+/-}$ and WT P14 T cells at d30 after acute or chronic LCMV infection. A decrease in IRF4 dosage resulted in a loss of large parts of the transcriptional signature associated with chronic infection and was sufficient for T cells to adopt a transcriptional profile similar to the one induced after acute infection (Figures 6A and S6A, Table S4). Although some memory T cell-associated genes were upregulated in *Irf4*$^{+/-}$ P14 T cells as early as d8 after infection, the majority of these genes were expressed at higher levels only at later time points (Figure S6A). *Irf4*$^{+/-}$ P14 T cells showed reduced transcript abundance for genes encoding inhibitory receptors, including *Havcr2*, *Tigit*, *Cd244*, *Pdcd1*, *Lag3*, and transcriptional regulators usually expressed at high amounts in exhausted cells, including *Prdm1* and *Maf* (Figure 6A). In contrast, *Irf4*$^{+/-}$ P14 T cells upregulated multiple genes associated with memory T cell development, including *Tcf7*, *Ccr7*, *Il7r*, and *Sell* (Figure 6A). Overall, 49% of the chronic signature genes were responsive to changes in IRF4 expression (Figure 6B, Table S5). Gene set enrichment analyses confirmed that expression of chronic signature genes was reduced, while expression of genes associated with memory T cell development was enriched in *Irf4*$^{+/-}$ compared to WT P14 T cells responding to chronic LCMV Docile (Figures 6C and 6D). Consistent with our observation that *Irf4* haploinsufficieny restored cellular metabolism during chronic infection, *Irf4*$^{+/-}$ P14 T cells showed higher expression of genes involved in OXPHOS, amino acid metabolism, fatty acid oxidation, the tricarboxylic acid cycle, and mitochondrial respiratory chain complexes (Figures 6E and 6F). Expression of *Aqp9*, a gene critical for memory T cell development and strongly downregulated in exhausted T cells, was recovered in *Irf4*$^{+/-}$ P14 T cells (Cui et al., 2015). Collectively, these data reveal that high amounts of IRF4 drive the transcriptional profile associated with CD8$^+$ T cell exhaustion.

High Amounts of IRF4 Repress Memory T Cell Development

Recently, we and others have shown that a population of antigen-specific T cells during chronic infection displays a memory-like phenotype and maintains the proliferative potential of exhausted T cells (He et al., 2016; Im et al., 2016; Leong et al.,

(B) Venn diagram showing significant overlap between "chronic CD8$^+$ T cell signature" genes and genes bound by all three transcription factors, IRF4, BATF, and NFAT (Fisher's exact test).

(C) Gene set enrichment test showing the top 500 genes bound by all three transcription factors, IRF4, BATF, and NFAT, demonstrating enrichment of genes that are associated with "exhaustion." Significance was tested using Gene Set Test.

(D) Representative ChIP sequencing tracks showing composite binding of IRF4, BATF, and NFAT to chronic CD8$^+$ T cell signature genes *Havcr2* (encoding TIM-3), *Tcf7* (encoding TCF1), and *Hif1a*.

(E) Genome wide co-localization of BATF, IRF4, and NFAT. Histograms show normalized average tag density at indicated distance from the nearest neighbor as indicated.

(F) Histogram showing the IRF4 motif distribution relative to the NFAT motif (anchor) in BATF/IRF4/NFAT triple binding regions.

(G) Representative ChIP sequencing tracks showing composite binding of IRF4, BATF, and NFAT to chronic CD8$^+$ T cell signature gene *Nfatc1*.

(H) Western blot showing NFATc1, NFATc2, IRF4, and Actin (loading control) expression in WT and *Irf4*$^{-/-}$ CD8$^+$ T cells at indicated time points after activation with anti-CD3 and anti-CD28 antibodies. The arrow marks the short isoform of NFATc1.

Data in (A)–(G) are combined from two independent experiments. Data in (H) are representative of two independent experiments.

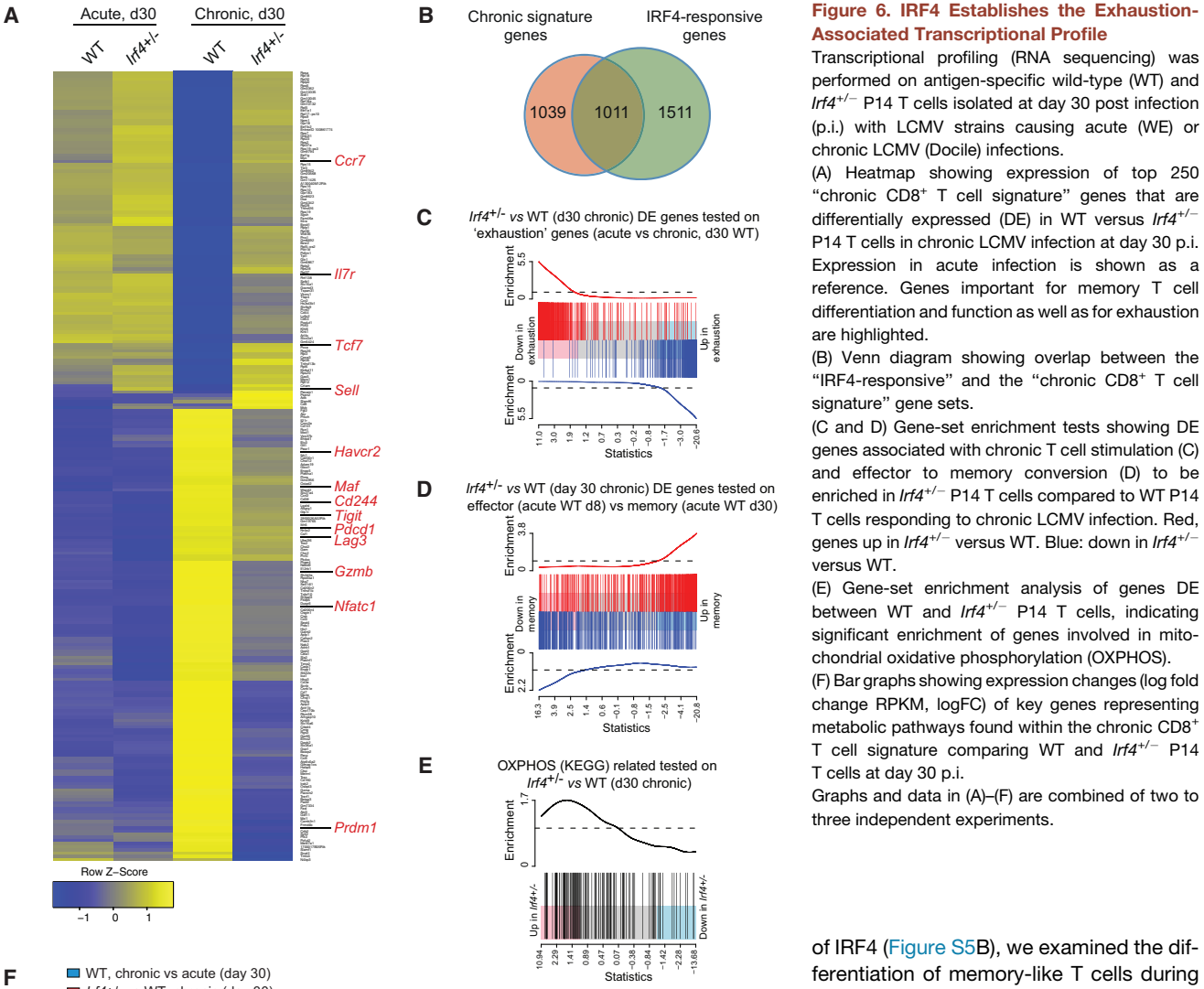

Figure 6. IRF4 Establishes the Exhaustion-Associated Transcriptional Profile

Transcriptional profiling (RNA sequencing) was performed on antigen-specific wild-type (WT) and *Irf4*$^{+/-}$ P14 T cells isolated at day 30 post infection (p.i.) with LCMV strains causing acute (WE) or chronic LCMV (Docile) infections.

(A) Heatmap showing expression of top 250 "chronic CD8^{+} T cell signature" genes that are differentially expressed (DE) in WT versus *Irf4*$^{+/-}$ P14 T cells in chronic LCMV infection at day 30 p.i. Expression in acute infection is shown as a reference. Genes important for memory T cell differentiation and function as well as for exhaustion are highlighted.

(B) Venn diagram showing overlap between the "IRF4-responsive" and the "chronic CD8^{+} T cell signature" gene sets.

(C and D) Gene-set enrichment tests showing DE genes associated with chronic T cell stimulation (C) and effector to memory conversion (D) to be enriched in *Irf4*$^{+/-}$ P14 T cells compared to WT P14 T cells responding to chronic LCMV infection. Red, genes up in *Irf4*$^{+/-}$ versus WT. Blue: down in *Irf4*$^{+/-}$ versus WT.

(E) Gene-set enrichment analysis of genes DE between WT and *Irf4*$^{+/-}$ P14 T cells, indicating significant enrichment of genes involved in mitochondrial oxidative phosphorylation (OXPHOS).

(F) Bar graphs showing expression changes (log fold change RPKM, logFC) of key genes representing metabolic pathways found within the chronic CD8^{+} T cell signature comparing WT and *Irf4*$^{+/-}$ P14 T cells at day 30 p.i.

Graphs and data in (A)–(F) are combined of two to three independent experiments.

2016; Utzschneider et al., 2016). These cells display increased expression of TCF1, Id3, and chemokine receptor CXCR5 and show reduced expression of TIM-3 and Blimp-1, consistent with the transcriptional profile of *Irf4*$^{+/-}$ P14 T cells. As we observed that *Tcf7*, which encodes TCF1, was a direct target of IRF4 (Figure S5B), we examined the differentiation of memory-like T cells during chronic infection in more detail. A much larger proportion of adoptively transferred *Irf4*$^{+/-}$ P14 T cells expressed TCF1 and CD62L, which correlated inversely with TIM-3 expression. In addition, these cells also expressed elevated amounts of CXCR5 and IL-7R compared to WT cells (Figures 7A–7C). Increased proportions of memory-like *Irf4*$^{+/-}$ P14 cells were established early and maintained throughout infection (Figure S6B). Although the proportion of TCF1^{+} cells was much increased among *Irf4*$^{+/-}$ P14 T cells, the overall numbers of both TCF1^{+} and TCF1^{-} *Irf4*$^{+/-}$ P14 T cells were reduced due to the critical role of IRF4 in T cell population expansion (Figure 7D). However, the reduction was much more substantial for TCF1^{-} cells, indicating that IRF4 specifically promotes the differentiation of fully exhausted T cells (Figure 7E).

To functionally test the recall capacity of chronically stimulated antigen-specific T cells expressing different amounts of IRF4, we

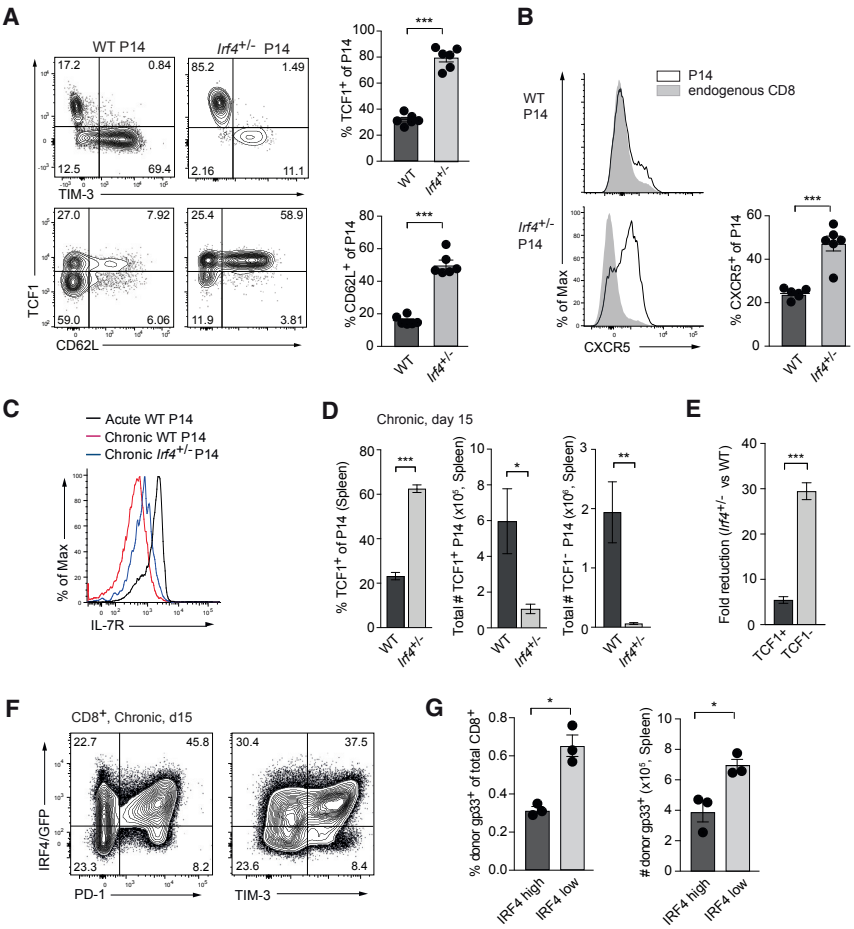

Figure 7. IRF4 Represses Memory T Cell Development

(A) Representative flow cytometry plots (left) showing TCF1 versus TIM-3 and CD62L on wild-type (WT) and *Irf4*$^{+/-}$ P14 cells isolated at day 13 post chronic LCMV (Docile) infection and enumeration (right).

(B) Representative histograms showing CXCR5 expression (left) on wild-type (WT) or *Irf4*$^{+/-}$ P14 cells in chronically LCMV-infected mice at day 13 post infection (p.i.) and enumeration (right).

(C) Expression of memory marker IL-7Rα on WT or *Irf4*$^{+/-}$ P14 cells in chronically or acutely LCMV-infected mice as indicated at day 30 p.i.

(D) Relative and absolute abundance of TCF1^{+} (left, middle) and TCF1^{-} (right) P14 cells at day 15 after chronic LCMV infection.

(E) Ratio of *Irf4*$^{+/-}$ versus WT P14 TCF1^{+} and TCF1^{-} cells, respectively, as in (D).

(F) Representative flow cytometry plots showing expression of IRF4/GFP versus PD-1 and TIM-3 in CD8 T cells in chronically LCMV-infected IRF4-reporter mice at day 15 p.i.

(G) Recall capacity of IRF4^{hi} or IRF4^{lo} gp33-specific T cells flow cytometry-sorted from IRF4 reporter mice at day 13 after chronic LCMV infection and transferred into congenically marked recipient mice infected with acute LCMV (WE) one day earlier. Proportions (left) and numbers (right) of donor cells at day 7 after transfer.

Data in (A)–(C) are representative of two to four independent experiments containing three to six mice per group. Data in (D), (E), and (G) are representative of two experiments containing three mice each. Error bars denote mean ± SEM and statistical analysis was performed using unpaired two-tailed Student's t test (*p < 0.05, **p < 0.01, ***p < 0.001).

made use of a newly developed reporter mouse that expresses green fluorescent protein (GFP) from the *Irf4* locus (Figure S6C). Chronically LCMV Docile-infected IRF4-reporter mice expressed high amounts of GFP in CD8^{+} T cells positive for PD-1 and TIM-3 (Figure 7F). However, a small proportion (15%–20%) of PD-1^{+}CD8^{+} T cells expressed low amounts of IRF4/GFP (Figure 7F). Notably, IRF4/GFP^{lo} gp33^{+}CD8^{+} T cells sorted from Docile-infected IRF4-reporter mice and adoptively transferred into acutely LCMV WE-infected host mice displayed greater proliferative potential compared to their IRF4/GFP^{hi} counterparts (Figure 7G). Overall, these data show that high amounts of IRF4 limit the memory potential of chronically stimulated antigen-specific T cells by directly repressing *Tcf7*.

DISCUSSION

The transcriptional program underlying CD8^{+} T cell exhaustion in response to chronic infection or tumor growth is incompletely known. Here we show that a network of TCR-dependent transcription factors consisting of IRF4, BATF, and NFATc1 was central for establishing T cell exhaustion during chronic infection. We demonstrate that IRF4 contributed to multiple aspects of T cell exhaustion, including inhibitory receptor expression, impaired cytokine secretion, and the repression of anabolic metabolism. High amounts of IRF4 also limited the development of memory-like T cells that are required for the replenishment of effector T cells in situations of persistent antigen stimulation and mediate the reinvigoration of T cells in response to checkpoint blockade.

IRF4 is a TCR signaling-sensitive transcription factor, which plays essential roles in acute CD8^{+} T cell responses by linking anabolic metabolism with clonal population expansion and effector T cell differentiation (Man and Kallies, 2015; Man et al., 2013). We show here that during chronic infection, IRF4 played a more complex role. While IRF4 was required for the initial expansion and subsequent maintenance of antigen-specific T cells during chronic infection, high amounts of IRF4 were central to establishing cardinal features of T cell exhaustion, including high expression of inhibitory receptors such as PD-1, TIM-3, and Lag3, altered cellular metabolism, and impaired cytokine secretion. Reducing the dosage of IRF4 resulted in decreased expression of inhibitory receptors, led to an overall increase in anabolic metabolism, and resulted in partially restored secretion of IFN-γ. Expression of high amounts of IRF4 was a physiological feature of exhausted T cells that was required to limit immune pathology. Thus, IRF4 expression needs to be finely balanced to maintain the proliferative capacity of antigen-specific T cells on the one side and limit their effector function during conditions of chronic antigen exposure on the other side.

Further analyses showed that IRF4 acted together with AP-1 factor BATF and NFAT, two transcription factors previously

implicated in promoting exhaustion and *Pdcd1* transcription (Martinez et al., 2015; Oestreich et al., 2008; Quigley et al., 2010). Together with IRF4 and BATF, the short isoform of NFATc1, known as NFATc1/αA, was upregulated in exhausted T cells, suggesting that NFATc1 and not NFATc2 is the dominant NFAT family member involved in exhaustion. This finding is in line with recent reports (Philip et al., 2017; Tirosh et al., 2016) that found NFATc1 was highly expressed in tumor-infiltrating T cells and played a critical role in driving cytotoxic T cell differentiation in acute infection (Klein-Hessling et al., 2017). NFATc1 expression was also found to promote IRF4 expression in follicular helper T cells (Vaeth et al., 2016), while *in vitro* experiments had shown that NFATc2 can bind to the *Irf4* locus (Martinez et al., 2015). These data are consistent with our results, which show that both NFATc1 and NFATc2 drive IRF4 expression in $CD8^+$ T cells during acute and chronic infection. Notably, both IRF4 and BATF also contributed to NFATc1 expression. IRF4 together with BATF bound to an intragenic region of *Nfatc1* and was required for the efficient expression of NFATc1/αA. Thus, together with the observation that NFATc1/αA expression is driven by its own promoter and amplified in an autoregulatory loop (Serfling et al., 2012), our data indicate that IRF4, BATF, and NFAT participate in a self-reinforcing transcriptional circuit that establishes the transcriptional network promoting T cell exhaustion during chronic infection.

Collaborative activity and co-binding of NFAT and IRF4 has been reported previously for individual target genes (Farrow et al., 2011; Hu et al., 2002; Lee et al., 2009; Rengarajan et al., 2002). Similarly, AP-1 binding sites were found to be enriched in an NFAT ChIP-seq analysis (Martinez et al., 2015). We found that in $CD8^+$ T cells, IRF4, BATF, and NFAT were recruited to adjacent binding sites, and binding of all three factors was significantly enriched among the core group of genes related to exhaustion, including *Pdcd1*, *Lag3*, *Havcr2*, *Tigit*, and *Ctla4.* Thus, in addition to AP1-IRF4 composite elements (AICE) that play important roles in T cell biology, our data indicate that NFAT_AP-1_IRF4 composite elements (NAICE) are particularly enriched among the genes regulating $CD8^+$ T cell exhaustion and may indeed be common among genes that play critical roles in T cell biology. Indeed, our data provide evidence that the IRF4, BATF, and NFAT transcription factor triplet directly bound and repressed the expression of *Tcf7*, encoding TCF1, which plays a critical role in the establishment of long-term memory T cells (Jeannet et al., 2010; Zhou et al., 2010). TCF1 is tightly downregulated in terminally differentiated and exhausted T cells; however, its expression is preserved in memory-like T cells during chronic infection and is required to maintain their proliferative potential (He et al., 2016; Im et al., 2016; Leong et al., 2016; Utzschneider et al., 2016). Importantly, downregulation of IRF4 was sufficient to release *Tcf7* from repression, allowing the development of memory-like T cells despite persistent viremia during chronic infection.

In summary, our findings reveal that the TCR-responsive transcription factors IRF4, BATF, and NFAT converge to establish the molecular characteristics of exhaustion, including the expression of inhibitory receptors. Furthermore, they act to restrain anabolic and mitochondrial metabolism, limit continued effector function, and oppose the development of memory-like cells during chronic T cell stimulation. Future studies will be required to determine how modulation of TCR-responsive transcription factors, inhibitory receptor signaling, and cellular metabolism can be combined to reverse immune dysfunction during chronic infection or cancer.

STAR★METHODS

Detailed methods are provided in the online version of this paper and include the following:

- KEY RESOURCES TABLE
- CONTACT FOR REAGENT AND RESOURCE SHARING
- EXPERIMENTAL MODEL AND SUBJECT DETAILS
  - Mice
  - IRF4 reporter mice
- METHOD DETAILS
  - Infections, adoptive cell transfer and viral titer determination
  - Histology
  - Tetramer, surface and intracellular staining and flow cytometry
  - Retroviral transduction of IRF4
  - Metabolic Assays
  - Real Time PCR analysis
  - Chromatin Immunoprecipitation (ChIP) and ChIPseq analysis
  - Transcriptome analysis
  - Gene Ontology Pathway Analysis and Gene Set Tests
  - Immunoblotting
- QUANTIFICATION AND STATISTICAL ANALYSIS
- DATA AND SOFTWARE AVAILABILITY

SUPPLEMENTAL INFORMATION

Supplemental Information includes six figures and five tables and can be found with this article online at https://doi.org/10.1016/j.immuni.2017.11.021.

AUTHOR CONTRIBUTIONS

K.M. designed the study, performed experiments, analyzed and interpreted data, and wrote the manuscript. S.S.G. contributed to the design of the study, performed experiments, analyzed and interpreted data, and wrote the manuscript. Y.L. and W.S. performed all bioinformatics analysis. R.G., S.P., and D.C.H. performed experiments. M.P., D.Z., F.B.-S., and M.A.F. contributed to the study design and interpretation of results. A.K. designed the study, analyzed and interpreted data, and wrote the manuscript.

ACKNOWLEDGMENTS

We wish to thank Liana Mackiewicz, Carolina Alvarado, and Benjamin Lunz for expert technical support, and Stephen Nutt, Edgar Serfling, and Stefan Klein-Hessling for scientific discussion. We thank Anjana Rao, Laurie Glimcher, Pamela Ohashi, Tak Mak, Ulf Klein, Mark Chong, and Daniel Gray for mice. This work was supported by grants and fellowships from the National Health and Medical Research Council of Australia (project grants 1032850 and 1085151 to A.K., 1006592, 1045549, and 1065626 to M.P., 1023454 to W.S., Senior Research Fellowship 1021168 and Senior Principal Research Fellowship 1116936 to M.A.F.), the Walter and Eliza Hall Institute Centenary Fellowship funded by CSL (to W.S.), the Swiss National Science Foundation and the Novartis Foundation for Medical-Biological Research (fellowships to S.S.G.), and the Sylvia and Charles Viertel Foundation (Senior Medical Research Fellowships to A.K. and M.P.). Further funding was provided by the Fritz Thyssen Stiftung (10.13.2.215) and the Wilhelm Sander-Stiftung (2012.047.1)

to F.B.-S. This study was made possible through Victorian State Government Operational Infrastructure Support and Australian Government NHMRC Independent Research Institute Infrastructure Support scheme.

Received: August 19, 2016
Revised: August 8, 2017
Accepted: November 28, 2017
Published: December 12, 2017

REFERENCES

Bengsch, B., Johnson, A.L., Kurachi, M., Odorizzi, P.M., Pauken, K.E., Attanasio, J., Stelekati, E., McLane, L.M., Paley, M.A., Delgoffe, G.M., and Wherry, E.J. (2016). Bioenergetic insufficiencies due to metabolic alterations regulated by the inhibitory receptor PD-1 are an early driver of CD8(+) T cell exhaustion. Immunity *45*, 358–373.

Blackburn, S.D., Shin, H., Haining, W.N., Zou, T., Workman, C.J., Polley, A., Betts, M.R., Freeman, G.J., Vignali, D.A., and Wherry, E.J. (2009). Coregulation of CD8+ T cell exhaustion by multiple inhibitory receptors during chronic viral infection. Nat. Immunol. *10*, 29–37.

Chang, C.H., Qiu, J., O'Sullivan, D., Buck, M.D., Noguchi, T., Curtis, J.D., Chen, Q., Gindin, M., Gubin, M.M., van der Windt, G.J., et al. (2015). Metabolic competition in the tumor microenvironment is a driver of cancer progression. Cell *162*, 1229–1241.

Cui, G., Staron, M.M., Gray, S.M., Ho, P.C., Amezquita, R.A., Wu, J., and Kaech, S.M. (2015). IL-7-induced glycerol transport and TAG synthesis promotes memory CD8+ T cell longevity. Cell *161*, 750–761.

Doedens, A.L., Phan, A.T., Stradner, M.H., Fujimoto, J.K., Nguyen, J.V., Yang, E., Johnson, R.S., and Goldrath, A.W. (2013). Hypoxia-inducible factors enhance the effector responses of CD8(+) T cells to persistent antigen. Nat. Immunol. *14*, 1173–1182.

Doering, T.A., Crawford, A., Angelosanto, J.M., Paley, M.A., Ziegler, C.G., and Wherry, E.J. (2012). Network analysis reveals centrally connected genes and pathways involved in CD8+ T cell exhaustion versus memory. Immunity *37*, 1130–1144.

Farrow, M.A., Kim, E.Y., Wolinsky, S.M., and Sheehy, A.M. (2011). NFAT and IRF proteins regulate transcription of the anti-HIV gene, APOBEC3G. J. Biol. Chem. *286*, 2567–2577.

Glasmacher, E., Agrawal, S., Chang, A.B., Murphy, T.L., Zeng, W., Vander Lugt, B., Khan, A.A., Ciofani, M., Spooner, C.J., Rutz, S., et al. (2012). A genomic regulatory element that directs assembly and function of immune-specific AP-1-IRF complexes. Science *338*, 975–980.

Griffon, A., Barbier, Q., Dalino, J., van Helden, J., Spicuglia, S., and Ballester, B. (2015). Integrative analysis of public ChIP-seq experiments reveals a complex multi-cell regulatory landscape. Nucleic Acids Res. *43*, e27.

Gubin, M.M., Zhang, X., Schuster, H., Caron, E., Ward, J.P., Noguchi, T., Ivanova, Y., Hundal, J., Arthur, C.D., Krebber, W.J., et al. (2014). Checkpoint blockade cancer immunotherapy targets tumour-specific mutant antigens. Nature *515*, 577–581.

He, R., Hou, S., Liu, C., Zhang, A., Bai, Q., Han, M., Yang, Y., Wei, G., Shen, T., Yang, X., et al. (2016). Follicular CXCR5- expressing CD8(+) T cells curtail chronic viral infection. Nature *537*, 412–428.

Heinz, S., Benner, C., Spann, N., Bertolino, E., Lin, Y.C., Laslo, P., Cheng, J.X., Murre, C., Singh, H., and Glass, C.K. (2010). Simple combinations of lineage-determining transcription factors prime cis-regulatory elements required for macrophage and B cell identities. Mol. Cell *38*, 576–589.

Ho, P.C., Bihuniak, J.D., Macintyre, A.N., Staron, M., Liu, X., Amezquita, R., Tsui, Y.C., Cui, G., Micevic, G., Perales, J.C., et al. (2015). Phosphoenolpyruvate is a metabolic checkpoint of anti-tumor T cell responses. Cell *162*, 1217–1228.

Hodge, M.R., Ranger, A.M., Charles de la Brousse, F., Hoey, T., Grusby, M.J., and Glimcher, L.H. (1996). Hyperproliferation and dysregulation of IL-4 expression in NF-ATp-deficient mice. Immunity *4*, 397–405.

Hu, C.M., Jang, S.Y., Fanzo, J.C., and Pernis, A.B. (2002). Modulation of T cell cytokine production by interferon regulatory factor-4. J. Biol. Chem. *277*, 49238–49246.

Huang, W., Sherman, B.T., and Lempicki, R.A. (2009). Systematic and integrative analysis of large gene lists using DAVID bioinformatics resources. Nat. Protoc. *4*, 44–57.

Im, S.J., Hashimoto, M., Gerner, M.Y., Lee, J., Kissick, H.T., Burger, M.C., Shan, Q., Hale, J.S., Lee, J., Nasti, T.H., et al. (2016). Defining CD8+ T cells that provide the proliferative burst after PD-1 therapy. Nature *537*, 417–421.

Jeannet, G., Boudousquié, C., Gardiol, N., Kang, J., Huelsken, J., and Held, W. (2010). Essential role of the Wnt pathway effector Tcf-1 for the establishment of functional CD8 T cell memory. Proc. Natl. Acad. Sci. USA *107*, 9777–9782.

Kahan, S.M., Wherry, E.J., and Zajac, A.J. (2015). T cell exhaustion during persistent viral infections. Virology *479-480*, 180–193.

Kao, C., Oestreich, K.J., Paley, M.A., Crawford, A., Angelosanto, J.M., Ali, M.A., Intlekofer, A.M., Boss, J.M., Reiner, S.L., Weinmann, A.S., and Wherry, E.J. (2011). Transcription factor T-bet represses expression of the inhibitory receptor PD-1 and sustains virus-specific CD8+ T cell responses during chronic infection. Nat. Immunol. *12*, 663–671.

Keir, M.E., Butte, M.J., Freeman, G.J., and Sharpe, A.H. (2008). PD-1 and its ligands in tolerance and immunity. Annu. Rev. Immunol. *26*, 677–704.

Klein, U., Casola, S., Cattoretti, G., Shen, Q., Lia, M., Mo, T., Ludwig, T., Rajewsky, K., and Dalla-Favera, R. (2006). Transcription factor IRF4 controls plasma cell differentiation and class-switch recombination. Nat. Immunol. *7*, 773–782.

Klein-Hessling, S., Muhammad, K., Klein, M., Pusch, T., Rudolf, R., Flöter, J., Qureischi, M., Beilhack, A., Vaeth, M., Kummerow, C., et al. (2017). NFATc1 controls the cytotoxicity of CD8+ T cells. Nat. Commun. *8*, 511.

Kurachi, M., Barnitz, R.A., Yosef, N., Odorizzi, P.M., Dilorio, M.A., Lemieux, M.E., Yates, K., Godec, J., Klatt, M.G., Regev, A., et al. (2014). The transcription factor BATF operates as an essential differentiation checkpoint in early effector CD8+ T cells. Nat. Immunol. *15*, 373–383.

Law, C.W., Chen, Y., Shi, W., and Smyth, G.K. (2014). voom: Precision weights unlock linear model analysis tools for RNA-seq read counts. Genome Biol. *15*, R29.

Lee, C.G., Kang, K.H., So, J.S., Kwon, H.K., Son, J.S., Song, M.K., Sahoo, A., Yi, H.J., Hwang, K.C., Matsuyama, T., et al. (2009). A distal cis-regulatory element, CNS-9, controls NFAT1 and IRF4-mediated IL-10 gene activation in T helper cells. Mol. Immunol. *46*, 613–621.

Leong, Y.A., Chen, Y., Ong, H.S., Wu, D., Man, K., Deleage, C., Minnich, M., Meckiff, B.J., Wei, Y., Hou, Z., et al. (2016). CXCR5(+) follicular cytotoxic T cells control viral infection in B cell follicles. Nat. Immunol. *17*, 1187–1196.

Li, P., Spolski, R., Liao, W., Wang, L., Murphy, T.L., Murphy, K.M., and Leonard, W.J. (2012). BATF-JUN is critical for IRF4-mediated transcription in T cells. Nature *490*, 543–546.

Liao, Y., Smyth, G.K., and Shi, W. (2013). The Subread aligner: fast, accurate and scalable read mapping by seed-and-vote. Nucleic Acids Res. *41*, e108.

Liao, Y., Smyth, G.K., and Shi, W. (2014). featureCounts: an efficient general purpose program for assigning sequence reads to genomic features. Bioinformatics *30*, 923–930.

Lu, P., Youngblood, B.A., Austin, J.W., Mohammed, A.U., Butler, R., Ahmed, R., and Boss, J.M. (2014). Blimp-1 represses CD8 T cell expression of PD-1 using a feed-forward transcriptional circuit during acute viral infection. J. Exp. Med. *211*, 515–527.

Man, K., and Kallies, A. (2015). Synchronizing transcriptional control of T cell metabolism and function. Nat. Rev. Immunol. *15*, 574–584.

Man, K., Miasari, M., Shi, W., Xin, A., Henstridge, D.C., Preston, S., Pellegrini, M., Belz, G.T., Smyth, G.K., Febbraio, M.A., et al. (2013). The transcription factor IRF4 is essential for TCR affinity-mediated metabolic programming and clonal expansion of T cells. Nat. Immunol. *14*, 1155–1165.

Martinez, G.J., Pereira, R.M., Äijö, T., Kim, E.Y., Marangoni, F., Pipkin, M.E., Togher, S., Heissmeyer, V., Zhang, Y.C., Crotty, S., et al. (2015). The transcription factor NFAT promotes exhaustion of activated CD8$^+$ T cells. Immunity *42*, 265–278.

Mittrücker, H.W., Matsuyama, T., Grossman, A., Kündig, T.M., Potter, J., Shahinian, A., Wakeham, A., Patterson, B., Ohashi, P.S., and Mak, T.W. (1997). Requirement for the transcription factor LSIRF/IRF4 for mature B and T lymphocyte function. Science *275*, 540–543.

Oestreich, K.J., Yoon, H., Ahmed, R., and Boss, J.M. (2008). NFATc1 regulates PD-1 expression upon T cell activation. J. Immunol. *181*, 4832–4839.

Paley, M.A., Kroy, D.C., Odorizzi, P.M., Johnnidis, J.B., Dolfi, D.V., Barnett, B.E., Bikoff, E.K., Robertson, E.J., Lauer, G.M., Reiner, S.L., and Wherry, E.J. (2012). Progenitor and terminal subsets of CD8+ T cells cooperate to contain chronic viral infection. Science *338*, 1220–1225.

Pearce, E.L., Poffenberger, M.C., Chang, C.H., and Jones, R.G. (2013). Fueling immunity: insights into metabolism and lymphocyte function. Science *342*, 1242454.

Pellegrini, M., Calzascia, T., Toe, J.G., Preston, S.P., Lin, A.E., Elford, A.R., Shahinian, A., Lang, P.A., Lang, K.S., Morre, M., et al. (2011). IL-7 engages multiple mechanisms to overcome chronic viral infection and limit organ pathology. Cell *144*, 601–613.

Philip, M., Fairchild, L., Sun, L., Horste, E.L., Camara, S., Shakiba, M., Scott, A.C., Viale, A., Lauer, P., Merghoub, T., et al. (2017). Chromatin states define tumour-specific T cell dysfunction and reprogramming. Nature *545*, 452–456.

Pircher, H., Ohashi, P., Miescher, G., Lang, R., Zikopoulos, A., Bürki, K., Mak, T.W., MacDonald, H.R., and Hengartner, H. (1990). T cell receptor (TcR) beta chain transgenic mice: studies on allelic exclusion and on the TcR+ gamma/delta population. Eur. J. Immunol. *20*, 417–424.

Quigley, M., Pereyra, F., Nilsson, B., Porichis, F., Fonseca, C., Eichbaum, Q., Julg, B., Jesneck, J.L., Brosnahan, K., Imam, S., et al. (2010). Transcriptional analysis of HIV-specific CD8+ T cells shows that PD-1 inhibits T cell function by upregulating BATF. Nat. Med. *16*, 1147–1151.

Rengarajan, J., Mowen, K.A., McBride, K.D., Smith, E.D., Singh, H., and Glimcher, L.H. (2002). Interferon regulatory factor 4 (IRF4) interacts with NFATc2 to modulate interleukin 4 gene expression. J. Exp. Med. *195*, 1003–1012.

Ritchie, M.E., Phipson, B., Wu, D., Hu, Y., Law, C.W., Shi, W., and Smyth, G.K. (2015). limma powers differential expression analyses for RNA-sequencing and microarray studies. Nucleic Acids Res. *43*, e47.

Sawada, S., Scarborough, J.D., Killeen, N., and Littman, D.R. (1994). A lineage-specific transcriptional silencer regulates CD4 gene expression during T lymphocyte development. Cell *77*, 917–929.

Schraml, B.U., Hildner, K., Ise, W., Lee, W.L., Smith, W.A., Solomon, B., Sahota, G., Sim, J., Mukasa, R., Cemerski, S., et al. (2009). The AP-1 transcription factor Batf controls T(H)17 differentiation. Nature *460*, 405–409.

Schurich, A., Pallett, L.J., Jajbhay, D., Wijngaarden, J., Otano, I., Gill, U.S., Hansi, N., Kennedy, P.T., Nastouli, E., Gilson, R., et al. (2016). Distinct metabolic requirements of exhausted and functional virus-specific CD8 T cells in the same host. Cell Rep. *16*, 1243–1252.

Seibler, J., Zevnik, B., Küter-Luks, B., Andreas, S., Kern, H., Hennek, T., Rode, A., Heimann, C., Faust, N., Kauselmann, G., et al. (2003). Rapid generation of inducible mouse mutants. Nucleic Acids Res. *31*, e12.

Sena, L.A., Li, S., Jairaman, A., Prakriya, M., Ezponda, T., Hildeman, D.A., Wang, C.R., Schumacker, P.T., Licht, J.D., Perlman, H., et al. (2013). Mitochondria are required for antigen-specific T cell activation through reactive oxygen species signaling. Immunity *38*, 225–236.

Serfling, E., Avots, A., Klein-Hessling, S., Rudolf, R., Vaeth, M., and Berberich-Siebelt, F. (2012). NFATc1/alphaA: The other face of NFAT factors in lymphocytes. Cell Commun. Signal. *10*, 16.

Shin, H., Blackburn, S.D., Intlekofer, A.M., Kao, C., Angelosanto, J.M., Reiner, S.L., and Wherry, E.J. (2009). A role for the transcriptional repressor Blimp-1 in CD8(+) T cell exhaustion during chronic viral infection. Immunity *31*, 309–320.

Smyth, G.K. (2004). Linear models and empirical bayes methods for assessing differential expression in microarray experiments. Stat. Appl. Genet. Mol. Biol. *3*, e3.

Speiser, D.E., Utzschneider, D.T., Oberle, S.G., Münz, C., Romero, P., and Zehn, D. (2014). T cell differentiation in chronic infection and cancer: functional adaptation or exhaustion? Nat. Rev. Immunol. *14*, 768–774.

Staron, M.M., Gray, S.M., Marshall, H.D., Parish, I.A., Chen, J.H., Perry, C.J., Cui, G., Li, M.O., and Kaech, S.M. (2014). The transcription factor FoxO1 sustains expression of the inhibitory receptor PD-1 and survival of antiviral CD8(+) T cells during chronic infection. Immunity *41*, 802–814.

Tirosh, I., Izar, B., Prakadan, S.M., Wadsworth, M.H., 2nd, Treacy, D., Trombetta, J.J., Rotem, A., Rodman, C., Lian, C., Murphy, G., et al. (2016). Dissecting the multicellular ecosystem of metastatic melanoma by single-cell RNA-seq. Science *352*, 189–196.

Utzschneider, D.T., Charmoy, M., Chennupati, V., Pousse, L., Ferreira, D.P., Calderon-Copete, S., Danilo, M., Alfei, F., Hofmann, M., Wieland, D., et al. (2016). T cell factor 1-expressing memory-like CD8(+) T cells sustain the immune response to chronic viral infections. Immunity *45*, 415–427.

Vaeth, M., Schliesser, U., Müller, G., Reissig, S., Satoh, K., Tuettenberg, A., Jonuleit, H., Waisman, A., Müller, M.R., Serfling, E., et al. (2012). Dependence on nuclear factor of activated T-cells (NFAT) levels discriminates conventional T cells from Foxp3+ regulatory T cells. Proc. Natl. Acad. Sci. USA *109*, 16258–16263.

Vaeth, M., Eckstein, M., Shaw, P.J., Kozhaya, L., Yang, J., Berberich-Siebelt, F., Clancy, R., Unutmaz, D., and Feske, S. (2016). Store-operated Ca(2+) entry in follicular T cells controls humoral immune responses and autoimmunity. Immunity *44*, 1350–1364.

Virgin, H.W., Wherry, E.J., and Ahmed, R. (2009). Redefining chronic viral infection. Cell *138*, 30–50.

Wang, R., and Green, D.R. (2012). Metabolic reprogramming and metabolic dependency in T cells. Immunol. Rev. *249*, 14–26.

Weinberg, S.E., Sena, L.A., and Chandel, N.S. (2015). Mitochondria in the regulation of innate and adaptive immunity. Immunity *42*, 406–417.

Wherry, E.J., and Kurachi, M. (2015). Molecular and cellular insights into T cell exhaustion. Nat. Rev. Immunol. *15*, 486–499.

Wherry, E.J., Ha, S.J., Kaech, S.M., Haining, W.N., Sarkar, S., Kalia, V., Subramaniam, S., Blattman, J.N., Barber, D.L., and Ahmed, R. (2007). Molecular signature of CD8+ T cell exhaustion during chronic viral infection. Immunity *27*, 670–684.

Wu, D., Lim, E., Vaillant, F., Asselin-Labat, M.L., Visvader, J.E., and Smyth, G.K. (2010). ROAST: rotation gene set tests for complex microarray experiments. Bioinformatics *26*, 2176–2182.

Yao, S., Buzo, B.F., Pham, D., Jiang, L., Taparowsky, E.J., Kaplan, M.H., and Sun, J. (2013). Interferon regulatory factor 4 sustains CD8(+) T cell expansion and effector differentiation. Immunity *39*, 833–845.

Zhou, X., Yu, S., Zhao, D.M., Harty, J.T., Badovinac, V.P., and Xue, H.H. (2010). Differentiation and persistence of memory CD8(+) T cells depend on T cell factor 1. Immunity *33*, 229–240.

STAR★METHODS

KEY RESOURCES TABLE

REAGENT or RESOURCE	SOURCE	IDENTIFIER
Antibodies		
Anti-CD8α (53-6.7)	Thermo Fisher Scientific	Cat#12-0081-82; RRID: AB_465530
Anti-CD44 (IM7)	BD Biosciences	Cat#553133; RRID: AB_2076224
Anti-CD62L (MEL-14)	Thermo Fisher Scientific	Cat#17-0621-82; RRID: AB_469410
Anti-CD71 (R17217)	Thermo Fisher Scientific	Cat#48-0711-82; RRID: AB_2574027
Anti-CD98 (RL388)	Thermo Fisher Scientific	Cat#12-0981-81; RRID: AB_465792
Anti-Ly5.1 (A20)	Thermo Fisher Scientific	Cat#45-0453-82; RRID: AB_1107003
Anti-Ly5.2 (104)	BD Biosciences	Cat#558702; RRID: AB_1645215
Anti-2B4 (eBio244F4)	Thermo Fisher Scientific	Cat#12-2441-82; RRID: AB_657872
Anti-PD-1 (J43)	Thermo Fisher Scientific	Cat#12-9985-82; RRID: AB_466295
Anti-Lag3 (T47-530)	Thermo Fisher Scientific	Cat#48-2231-82; RRID: AB_11149866
Anti-TIGIT (GIGD7)	Thermo Fisher Scientific	Cat#46-9501-82; RRID: AB_11150967
Anti-CTLA4 (14D3)	Thermo Fisher Scientific	Cat#106310; RRID: AB_2087653
Anti-CD127 (A7R34)	Thermo Fisher Scientific	Cat#45-1271-82; RRID: AB_1106998
Anti-CXCR5 (SPRCL5)	Thermo Fisher Scientific	Cat#46-7185-82; RRID: AB_2573837
Anti-TIM-3 (RMT3-23)	Thermo Fisher Scientific	Cat#119721; RRID: AB_2616907
Anti-IL-2 (JES6-5H4)	Thermo Fisher Scientific	Cat#45-7021-82; RRID: AB_925755
Anti-IFNγ (XMG1.2)	Thermo Fisher Scientific	Cat#11-7311-82; RRID: AB_465412
Anti-TNF (MP5-XT22)	BD Biosciences	Cat#554420; RRID: AB_398553
Anti-TCF1 (C63D9)	Cell Signaling Technology	Cat#2203; RRID: AB_2199302
Anti-BATF (D7C5)	Cell Signaling Technology	Cat#8638; RRID; AB_11141425
Anti-IRF4 (REA201)	Miltenyi	Cat# 130-100-921; RRID: AB_2652514
Anti-IRF4 (M-17)	Santa Cruz Biotechnology	Cat#sc-6059; RRID: AB_2127145
Anti-NFATc2 (D43B1)	Cell Signaling Technology	Cat#5861; RRID: AB_10835147
Anti-NFATc2 (25A10.D6.D2)	Abcam	Cat#ab2722; RRID: AB_303247
Anti-NFATc1 (7A6)	Abcam	Cat#ab2796; RRID: AB_303308
Anti-Actin (I-19)	Santa Cruz Biotechnology	Cat#sc-1616; RRID: AB_630836
Anti-p50 NF-κB (H-119)	Santa Cruz Biotechnology	Cat#sc-7178; RRID: AB_650211
Bacterial and Virus Strains		
Lymphocytic choriomeningitis Virus (LCMV) WE	Zinkernagel lab	generated in house
Lymphocytic choriomeningitis Virus (LCMV) Docile	Zinkernagel lab	generated in house
Chemicals, Peptides, and Recombinant Proteins		
LCMV–$gp_{33–41}$ (KAVYNFATM) tetramer	Baylor College of Medicine, MHC Tetramer Production Facility	N/A
LCMV–$NP_{396–404}$ (FQPQNGQFI) tetramer	Baylor College of Medicine, MHC Tetramer Production Facility	N/A
LCMV–$gp_{33–41}$ (KAVYNFATM) peptide	Anaspec	Cat#AS-61296
rhIL-2	Peprotech	Cat# 200-02
rmIL-15	Peprotech	Cat# 210-15
Sytox Blue Dead Cell Stain	Thermo Fisher Scientific	Cat#S34857
Fixable Viability Dye eFluor506	Thermo Fisher Scientific	Cat#65-0866-18
Critical Commercial Assays		
2-NBDG	Thermo Fisher Scientific	Cat#N13195
MitoTracker Green	Thermo Fisher Scientific	Cat#M7514
MitoTracker Orange CMTMRos	Thermo Fisher Scientific	Cat#M7510

(*Continued on next page*)

Continued

REAGENT or RESOURCE	SOURCE	IDENTIFIER
CellROX Deep Red	Thermo Fisher Scientific	Cat#C10491
Glycolysis Cell-Based Assay Kit	Cayman Chemical	Cat#600450
FoxP3 Transcription Factor Staining Buffer Kit	Thermo Fisher Scientific	Cat#A25866A
BD Cytofix/Cytoperm	BD Biosciences	Cat#554714
$CD8a^+$ T Cell Isolation Kit, mouse	Miltenyi	Cat#130-104-075
Anti-Biotin MicroBeads	Miltenyi	Cat#130-090-485
Seahorse XF Cell Mito Stress Test Kit	Agilent	Cat#103015-100
Cyclosporin A	Merck	Cat#30024
Deposited Data		
BATF ChIP, IRF4 ChIP	Kurachi et al. (2014)	GSE54191
NFATc2 ChIP	Martinez et al. (2015)	GSE64407
IRF4 ChIP	Man et al. (2013)	GSE49930
RNaseq (NFATc2KO and WT)	Martinez et al. (2015)	GSE64409
RNaseq (IRF4KO and WT)	Man et al. (2013)	GSE49929
Micorarray (BATFKO and WT)	Kurachi et al. (2014)	GSE54215
RNaseq (IRF4Het and WT)	this study	GSE84820
Experimental Models: Organisms/Strains		
Irf4$^{-/-}$	Lab of Tak Mak	Mittrücker et al. (1997)
Irf4$^{fl/fl}$	Lab of Ulf Klein	Klein et al. (2006)
Batf$^{-/-}$	The Jackson Laboratory	(B6.129S-*Batf*$^{tm1.1Kmm}$/J); Schraml et al. (2009)
Nfatc2$^{-/-}$	Lab of L. Glimcher	Hodge et al. (1996)
Nfatc1$^{fl/fl}$	Lab of A. Rao	Martinez et al. (2015)
P14ab TCR	Lab of P. Ohashi	Pircher et al. (1990)
CD4Cre	Lab of M. Chong	Sawada et al. (1994)
CreERT2	Artemis	Seibler et al. (2003)
Irf4GFP	Lab of A. Kallies; this paper	N/A
Oligonucleotides		
Irf4-Promoter-F (TGAAACCGCC TAAGTCAAGG) (ChIP)	Integrated DNA Technologies	N/A
Irf4-Promoter-R (GAACTATCC CGGTCACCAGA) (ChIP)	Integrated DNA Technologies	N/A
Pdcd1-CRB-F (GGCAGTGTCGC CTTCAGTAGC) (ChIP)	Integrated DNA Technologies	N/A
Pdcd1-CRB-R (CCACCTCTAGTT GCCTGTTCTC) (ChIP)	Integrated DNA Technologies	N/A
IRF4 F (TGCAAGCTCTTTGACACACA)	Integrated DNA Technologies	N/A
IRF4 R (CAAAGCACAGAGTCACCTGG)	Integrated DNA Technologies	N/A
Batf F (TGGCAAACAGGACTCATCTG)	Integrated DNA Technologies	N/A
Batf R (TGTCGGCTTTCTGTGTCTGT)	Integrated DNA Technologies	N/A
Hprt-F (GGGGGCTATAAGTTCTTTGC)	Integrated DNA Technologies	N/A
Hprt-R (TCCAACACTTCGAGAGGTCC)	Integrated DNA Technologies	N/A
Recombinant DNA		
pMSCV IRES-mCherry	In house	N/A
pMSCV IRF4-IRES-mCherry	In house	N/A
Software and Algorithms		
Graphpad Prism 7.0	https://www.graphpad.com	N/A
FlowJo 9 and 10	https://www.flowjo.com	N/A
Subread aligner	http://subread.sourceforge.net/	Liao et al. (2013)

(*Continued on next page*)

Continued

REAGENT or RESOURCE	SOURCE	IDENTIFIER
featureCounts	http://subread.sourceforge.net/	Liao et al. (2014)
limma	http://www.bioconductor.org/packages/release/bioc/html/limma.html	Ritchie et al. (2015)
Homer	http://homer.ucsd.edu/homer/	Heinz et al. (2010)

CONTACT FOR REAGENT AND RESOURCE SHARING

Further information and requests for resources and reagents should be directed to and will be fulfilled by the Lead Contact, Axel Kallies (kallies@wehi.edu.au).

EXPERIMENTAL MODEL AND SUBJECT DETAILS

Mice

Irf4$^{-/-}$, *Irf4*$^{fl/fl}$, *Batf*$^{-/-}$, *Nfatc1*$^{fl/fl}$ and *Nfatc2*$^{-/-}$ mice were described previously (Mittrücker et al., 1997; Klein et al., 2006; Schraml et al., 2009; Hodge et al., 1996; Martinez et al., 2015; Vaeth et al., 2012) and maintained on a C57BL/6 (Ly5.2) background. For some experiments mice were crossed to P14 TCR transgenic mice (Pircher et al., 1990), mice that expressed Cre recombinase under the control of the *Cd4* gene regulatory elements (*Cd4Cre*) (Sawada et al., 1994) or mice that have tamoxifen-inducible expression of Cre recombinase from the ubiquitous *Rosa26* locus (*Cre*ET2) (Seibler et al., 2003). Mixed bone marrow chimeras were generated from lethally irradiated (2 × 550 R) wild-type Ly5.1^{+}Ly5.2^{+} mice reconstituted with a mixture of congenically marked mutant and/or control bone marrow as indicated, and mice were allowed 6-8 weeks to reconstitute. Mice were maintained and used in accordance with the guidelines of the Walter and Eliza Hall Institute Animal Ethics Committee.

IRF4 reporter mice

The generation and characterization of the *Irf4*^{GFP} reporter mice will be published in detail elsewhere. Briefly, an internal ribosomal entry site (IRES) followed by an enhanced green fluorescence (eGFP) cassette was inserted 3′ of exon 8 of the *Irf4* gene. Correct targeting and Neo removal was confirmed by Long Range PCR and Southern Blot.

METHOD DETAILS

Infections, adoptive cell transfer and viral titer determination

Lymphocytic choriomeningitis virus (LCMV) WE and LCMV Docile strains were propagated on L929 cells. Frozen stocks were diluted in PBS and 3x10^{2}-1x10^{3} p.f.u. of LCMV WE or 2x10^{6} p.f.u. of LCMV Docile were administered intravenously. On the same or next day, 5x10^{2} to 5x10^{3} naive WT (Ly5.1), *Irf4*$^{+/-}$ or *Irf4*$^{-/-}$ (Ly5.2) P14 CD8^{+} T cells were adoptively transferred intravenously into infected congenically marked host mice. In most experiments, WT (Ly5.1) and *Irf4* mutant (Ly5.2) P14 cells were co-transferred into or Ly5.1/Ly5.2 hosts. In experiments designed to measure the pathogenic potential of P14 T cells, numbers of transferred cells were adjusted so that WT and *Irf4*$^{+/-}$ P14 cells reached similar numbers at day 13 post infection. Thus, 5x10^{3} WT P14 or 5x10^{4} *Irf4*$^{+/-}$ P14 were transferred and core body temperature of mice was measured daily. To determine viral titers, organs were homogenized using the QIAGEN Tissue Lyser and were quantified by focus-forming assays using MC57 fibroblast cells as previously described (Pellegrini et al., 2011).

Histology

Formalin fixed sections were stained with Eosin and Hematoxylin and scanned with an Aperio slide scanner (Leica).

Tetramer, surface and intracellular staining and flow cytometry

LCMV-specific CD8^{+} T cell responses were enumerated with MHC class I (H-2D^{b}) tetramers complexed with either LCMV–gp$_{33–41}$ (KAVYNFATM) or LCMV–NP$_{396–404}$ (FQPQNGQFI). T cell restimulations were performed using antigen-specific peptides (LCMV, gp$_{33-41}$) (10^{-7}M) in the presence of GolgiStop (BD Biosciences) for 5 hours. Intracellular staining of cytokines was performed using the BD Cytofix/Cytoperm kit, staining of transcription factor was performed using the FoxP3 staining kit (eBioscience) according to manufacturer's protocols.

Fluorochrome-conjugated antibodies directed against the following antigens were used for analysis by flow cytometry: CD8α (53-6.7), CD62L (MEL-14), CD71 (R17217), CD98 (RL388), Ly5.1 (A20), 2B4 (eBio244F4), PD-1 (J43), Lag3 (T47-530), TIGIT (GIGD7), CTLA4 (14D3), TIM-3 (RMT3-23), CD127 (A7R34), CXCR5 (SPRCL5), IL-2 (JES6-5H4), IFNγ (XMG1.2) (from Thermo Fisher Scientific), CD44 (IM7), Ly5.2 (104), TNF (MP5-XT22) (from BD Biosciences), IRF4 (REA201) (from Miltenyi), TCF1 (C63D9), BATF (D7C5) (from Cell Signaling Technology), IRF4 (M17) (from Santa Cruz Biotechnology), and anti-goat IgG coupled to fluorescein isothiocyanate (Jackson ImmunoResearch Laboratories) and anti-rabbit IgG coupled to Alexa Fluor 647 (Thermo Fisher Scientific).

Propidium iodide, SytoxBlue or fixable viability dye eFluor506 (all Thermo Fisher Scientific) were used to exclude dead cells. In some experiments, $CD8^+$ T cells were enriched prior to analysis by depletion using antibodies against CD11b (M1/70), F4/80 (F4/80), Ter-119, Gr-1 (RB6-8C5), MHCII (M5/114), and CD4 (GK1.5) (hybridoma supernatant, generated in house).

Retroviral transduction of IRF4

Retroviral supernatant was produced from HEK293 T cells transfected with retroviral expression plasmids (pMSCV) containing either an IRES-mCherry or IRF4-IRES-mCherry expression cassette. For retroviral transduction, naive $CD8^+$ T cells were isolated from spleens and lymph nodes of P14$\alpha\beta$ TCR transgenic mice and activated *in vitro* with gp_{33-41} peptide (KAVYNFATM) (100 ng/ml) in the presence of recombinant human IL-2 (30 U/ml, Peprotech) and IL-15 (20 ng/ml, Peprotech) for 48 hours before spin transduction with viral supernatants in the presence of 0.8 mg/ml polybrene. After 24 hours, $Cherry^+$ cells were obtained by fluorescence activated cell sorting (FACS) and $1x10^4$ cells were immediately transferred into $Ly5.1^+$ recipients which were infected with either LCMV WE or LCMV Docile the previous day.

Metabolic Assays

For extracellular flux assays, effector T cells ($CD3^+CD8^+CD44^+CD62L^-$) were obtained by flow-cytometry sorting from C57B/6J mice infected with LCMV WE or LCMV Docile at day 8 or day 30 post infection for directly assaying in at least triplicates with equal plating density in DMEM containing 1 mM L-Ala-Gln (glutamax), 1 mM sodium pyruvate and 25 mM glucose. Oxygen consumption rates (OCR) and extracellular acidification rates (ECAR) were measured at baseline and in response to Oligomycin, FCCP and rotenone/antimycin A according to manufacturer's protocols (Mito Stress Test Kit, Agilent) using the XF-96 Extracellular Flux Analyzer (Agilent).

To determine glucose uptake *ex vivo*, adoptively transferred WT and $Irf4^{+/-}$ P14$\alpha\beta$ T cells or tetramer specific $gp_{33-41}{}^+$ T cells from LCMV Docile infected host mice were incubated with 30 μM of a fluorescently labeled glucose analog (2-NBDG, Thermo Fisher Scientific) for 30 minutes in glucose-free RPMI and washed twice with PBS before staining with labeled antibodies against cell surface proteins. Mitochondrial mass was assessed by labeling with 100 nM Mitotracker Green, mitochondrial membrane potential with 200 nM of Mitotracker Orange CMTMRos, and reactive oxygen species (ROS) detected by labeling with 5 μM of CellRox DeepRed in complete media for 30 minutes at 37°C (all Thermo Fisher Scientific). Extracellular L-lactate concentration was determined *ex vivo* from FACS sorted WT P14 T cells from LMCV WE and LCMV Docile infected host mice, and were re-cultured overnight at equal density in complete media supplemented with recombinant human IL-2 (30 U/ml, Peprotech) before extracellular L-Lactate concentrations were determined using the Glycolysis Cell-Based Assay Kit (Cayman Chemical) according to manufacturer's protocols.

Real Time PCR analysis

Total RNA was prepared from flow cytometrically purified $gp33^+$ $CD8^+$ T cells using an RNeasy kit (QIAGEN). The cDNA was synthesized from total RNA with random hexamers and Superscript III reverse transcriptase (Invitrogen). Real-time PCR was performed using the QuantiTect SYBR Green PCR kit (QIAGEN).

Chromatin Immunoprecipitation (ChIP) and ChIPseq analysis

Effector $CD8^+$ T cells ($CD3^+CD8^+CD44^+CD62L^-$) were obtained by FACS sorting from C57B/6J mice infected with LCMV-WE or LCMV-Docile at day 8 post infection before immediate cross-linking by addition of 1% PFA at room temperature for 10 minutes, followed by sonication and immunoprecipitation with anti-NFATc2 (25A10.D6.D2), anti-NFATc1 (7A6) (Abcam), anti-IRF4 (M-17), or a corresponding rabbit polyclonal-IgG or mouse polyclonal IgG control antibodies (Santa Cruz Biotechnology). The precipitated DNA was quantified by real-time PCR analysis with SYBR green, which was carried out on a MyiQ instrument (Bio-Rad). Primer sequences were *Irf4*-Promoter-F, TGAAACCGCCTAAGTCAAGG; *Irf4*-Promoter-R, GAACTATCCCGGTCACCAGA; *Pdcd1*-Promoter-F, GGCAGTGTCGCCTTCAGTAGC; *Pdcd1*-Promoter-R, CCACCTCTAGTTGCCTGTTCTC.

ChIPseq data for IRF4, BATF and NFATc2 (NFAT1) were published previously (Kurachi et al., 2014; Man et al., 2013; Martinez et al., 2015) and were downloaded from the Gene Expression Omnibus (GEO) database (accession numbers GSE54191 GSE64407 and GSE49930). Two samples of the Martinez et al. (2015) study were used, GSM1570759 as NFAT-ChIP and GSM1570753 as input. Sequence reads were aligned to the GRCm38/mm10 build of the *Mus musculus* genome using the Subread aligner (Liao et al., 2013) and only uniquely mapped reads were retained. Binding peaks were called using the Homer program (Heinz et al., 2010). Chromatin input controls were used to test the significance of binding enrichment. FDR cutoffs applied for calling peaks for IRF4, BATF and NFATc2 were 1e-6, 1e-6 and 1e-12, respectively. Called peaks were assigned to a gene if they overlap with the body of the gene plus 20kb upstream and 5kb downstream regions. RefSeq mouse gene annotation (build 38.1) was used in assigning peaks to genes. Target genes were matched with genes included in RNA-seq expression data via Entrez gene identifier. Fisher's Exact test (two-sided) was performed to test the enrichment of binding target genes in the chronic signature.

To detect co-binding, we identified peaks that were overlapping by at least 1 bp as reported before (Griffon et al., 2015). We identified 2185 sites in which IRF4 ChIPseq peaks overlapped with both NFAT and BATF ChIPseq peaks (mean overlap > 113 bp). To detect exact binding motif sequences in the 3-cobinding sites, we extended the leftmost summit by 100 bp to the left and extended the rightmost summit by 100 bp to the right. To detect binding sites potentially shared by IRF4 and NFAT, we identified the NFAT core (GGAAA) and IRF4 core (GAAA) motifs closest to the IRF4 and NFAT ChIPseq peak summits. This identified 575 sites potentially

shared between IRF4 and NFAT. Distance plots are centered to the middle of the anchor sequence or anchor peak as indicated. For example, for the "IRF4 motif to NFAT motif (anchor)" plot, we located all the NFAT core sequences (the anchors) under the composite peak. We then located the nearest IRF4 motif for each of the anchor sequence and plotted the distance from the center of the anchor to the nearest base in the nearest IRF4 motif in the plot. De novo motif discovery was performed by selecting regions bound together by IRF4, BATF and NFAT. Motif discovery analysis was performed with MEME.

Transcriptome analysis

RNA sequencing reads were aligned to the GRCm38/mm10 build of the *Mus musculus* genome using the Subread aligner (Liao et al., 2013). Only uniquely mapped reads were retained. Genewise counts were obtained using featureCounts (Liao et al., 2014). Reads overlapping exons in annotation build 38.1 of NCBI RefSeq database were included. Genes were filtered from downstream analysis if they failed to achieve a CPM (counts per million mapped reads) value of at least 0.5 in at least one library. Counts were converted to log2 counts per million, quantile normalized and precision weighted with the 'voom' function of the limma package (Law et al., 2014; Ritchie et al., 2015). A linear model was fitted to each gene, and empirical Bayes moderated *t*-statistics were used to assess differences in expression (Smyth, 2004). P values from Bayes moderated t tests were adjusted to control the global false discovery rate (FDR) across all comparisons with the 'global' option of the limma package. Genes were called differentially expressed if they achieved a FDR of 0.1 or less and had an expression change of 1.5 folds or greater. The called differentially expressed genes must also have at least 8 RPKMs (reads per kilobase of exon length per million mapped reads) in one or both of the two cell types being compared.

We also analyzed two public datasets downloaded from the Gene Expression Omnibus (GEO) database. Dataset GSE54215 includes Affymetrix microarray data generated from wild-type and *Batf*$^{-/-}$ effector CD8^{+} T cells. Data were normalized using the Robust Multi-array Average (RMA) approach. Expression analysis was carried out using limma package. Linear models were fitted to gene expression data and empirical Bayes moderated *t*-statistics were used to assess differential expression. A gene must have a FDR value less than 0.15 to be called a differentially expressed gene. The other public dataset included in this study is an RNA-seq dataset with GEO accession number GSE64409, which was analyzed to discover genes regulated by NFAT in CD8^{+} T cells. This dataset was analyzed in a similar manner as the analysis of RNA-seq data generated in this study (see above). A gene is required to have a FDR value less than 0.25 and a fold-change greater than 1.5-fold to be called NFAT-regulated gene.

The 'IRF4-responsive' gene set was the combined list of genes identified as differentially expressed between WT and *Irf4*$^{-/-}$ OT-1 CD8^{+} T cells responding to high-affinity stimulation (GSE49929, Man et al., 2013) and genes differentially expressed between WT and *Irf4*$^{+/-}$ responding to LCMV infection identified in this study.

Gene Ontology Pathway Analysis and Gene Set Tests

The Database for Annotation, Visualization and Integrated Discovery (DAVID) (Huang et al., 2009) was used to identify enriched gene ontology terms based on our differentially expressed gene sets using the functional annotation clustering tool. Gene set enrichment plots were generated with the 'barcodeplot' function in the limma package. Statistical tests of enrichment were carried out using the 'roast' method in limma with 999 rotations (Wu et al., 2010). One-sided P values are reported.

Immunoblotting

CD8^{+} cells were either flow-cytometry sorted from mice at indicated time points post LCMV infection or purified from naive mice and stimulated with anti-CD3 and anti-CD28 antibodies for the indicated duration. In some cases, cultures were treated with 2 μg/ml cyclosporine A (LC Laboratories) as indicated. Whole cell extracts were produced by cell lysis in RIPA buffer containing standard protease inhibitors. Proteins were resolved by denaturing SDS-PAGE and transferred onto nitrocellulose membrane. The following primary antibodies were used anti-IRF4 (M-17), anti-Actin (I-19), anti-p50 NF-κB (H-119), anti-NFATc2 (D43B1), anti-BATF (D7C5) (Cell Signaling Technology) and anti-NFATc1 (7A6) (Abcam).

QUANTIFICATION AND STATISTICAL ANALYSIS

For statistical analysis, GraphPad Prism 7.0 was used. Two-tailed unpaired or paired Student's t test was used as indicated to test for statistical significance. *P*-values < 0.05 were considered significant (*p < 0.05; **p < 0.01; ***p < 0.001), p ≥ 0.05 not significant (N.S.). Error bars denote ± SEM.

DATA AND SOFTWARE AVAILABILITY

Gene Expression Omnibus: RNA sequencing data have been deposited under accession code GSE84820.